Hochschule Esslingen
University of Applied Sciences

Höganäs

Master Thesis

Integrating sensors in components using additive manufacturing

Magalie Darnis

16th February 2016

Design and Development in Automotive and Mechanical Engineering

Hochschule Esslingen – University of Applied Sciences

Magalie Darnis
ID-number: 00750281

Integrating sensors in components using additive manufacturing

1st supervisor:
Prof. Dr.-Ing. Peter Häfele
Hochschule Esslingen - University of Applied Sciences

2nd supervisor:
Michael Andersson PhD
Senior Engineer PM Components
Höganäs AB

Declaration of authenticity

Student: Magalie, Cécile, Marie DARNIS

ID-number: 00750281

Master Program: M.Eng. in Design and Development for Automotive and Mechanical Engineering

Title of Thesis: Integrating sensors in components using additive manufacturing

I hereby declare that I have written the attached work alone and without any other reference works than those mentioned. All thoughts or quotations taken directly or indirectly from other sources have been noted as such. Furthermore, I have not use this work, parts of this work or basic ideas from this work to achieve credits in any academic course at any time.

Darnis

16 / 02 / 2016

Signature

Date

Abstract

The scope of this thesis was to investigate the feasibility of building components with integrated sensors using additive manufacturing technologies.

Contrary to subtractive manufacturing processes, additive manufacturing aims to create a solid final part from a digital model by adding material. Enabling novel geometries and novel material combinations, these technologies are suitable when it comes to smart parts with embedded systems.

In order to investigate the possible alternatives, different designs were developed and produced using two different additive manufacturing processes and combination of materials. These printed designs were then categorised into four groups of sensors: deformation-, binary-, force- and vibration sensors.

The printability and the combination of material investigated in this thesis has proven that the working principles of the developed designs were suitable to create smart parts with embedded 3D printed sensors.

However there were some issues for 3D printed parts that needed to be dealt with. Generally, the material properties of a printed part was affected by a lot of factor. The profound influence of the printing direction led to design choices during the pre-printing phase and only experience has been helpful to narrow down their impacts. Besides, the designs exposed in this paper could as well be enhanced in order to enlarge the possible applications with a better accuracy and to overcome the manufacturing troubleshooting that may occur.

In spite all of it, the overall conclusion of this thesis work was that it is possible to integrate sensors in components using additive manufacturing.

Keywords: Additive manufacturing, smart parts, 3D printed sensors

Foreword

I express my gratitude to Michael Andersson, my supervisor at Höganäs AB, for his support and valuable advises during this project. I thank him for sharing his knowledge and giving me the chance to have my own experience.

I also would like to thank Anders Flodin, project manager in gear applications, for his useful remarks and proper guidance.

Many thanks also to Per Helgesson for being my go-to guy. His inputs were very useful and each of our conversations constructive. Thanks also for the help with all the experimental setups.

I would like to thank the Digital Metal® department of Höganäs AB and especially Marie Stensson for her efficiency and her help with the printing of my metal sensor, as well as Sara, Ida and Jelica for their patience while cleaning my parts.

Thanks also to Prof. Dr.-Ing. Peter Häfele from the Hochschule Esslingen for asking the right questions.

Also, I would like to thank all the people I met during this thesis for having the kindness to share their precious time and knowledge with me. Thanks as well to Sofia for the relevant comments throughout this work and the external perspective that pushed me to be clearer when writing this report.

Finally, I would like to take the occasion to tell to my parents, my brother and my sister, my relatives, my friends and all the people who one day helped me to achieve my goal how thankful I am. This Thesis work finalizes my Master course as well as my engineering studies. I could not have been successful without their support. Merci.

Table of Contents

Declaration of authenticity ii

Abstract iii

Foreword iv

List of abbreviations vii

List of figures ix

List of tables xi

1. Introduction 1
   - 1.1. Objectives 1
   - 1.2. Project plan 1
2. Literature review 3
   - 2.1. Additive Manufacturing (AM) 3
     - 2.1.1. Description of the AM process 3
     - 2.1.2. Additive manufacturing technologies 4
     - 2.1.3. Comparison of AM and conventional processes 11
   - 2.2. Industrie 4.0 14
   - 2.3. Sensors 16
3. Working equipment 18
   - 3.1. FlashForge Dreamer 18
   - 3.2. Software 19
4. Filaments characteristics 20
   - 4.1. Storage 20
   - 4.2. PolyLactic Acid (PLA) 20
   - 4.3. PI-ETPU 95-250 Carbon Black (ETPU) 22
     - 4.3.1. Characteristic temperatures 23
     - 4.3.2. Electrical resistivity 24

4.3.3. Relation between strain and variation of electrical resistance in printed ETPU material........29
4.3.4. Influence of the temperature on printed ETPU resistance........31
4.3.5. Density........33
4.3.6. Module of elasticity........33
5. Sensors........35
5.1. Deformation sensor........35
5.2. Binary sensor........40
5.3. Force sensor........44
5.4. Vibration sensor........46
5.4.1. ETPU/PLA sensor........48
5.4.2. Metal sensor........54
6. Discussions and conclusions........60
References........61
Appendices........65

List of abbreviations

.STL	Standard Tessellation Language
ABS	Acrylonitrile Butadiene Styrene
AM	Additive Manufacturing
CAD	Computer Aided Design
CPS	Cyber-Physical System
d	Density
DMLS	Direct Metal Laser Sintering
d_{printed}	Density of printed ETPU material
DSC	Differential Scanning Calorimetry
d_{SS}	Printed density of SS316L metal powder
$E_{\text{ETPU, filament}}$	Young’s modulus of ETPU filament
E_{printed}	Young’s modulus of printed ETPU material
E_{SS}	Young’s modulus of SS316L metal powder
ETPU	Electrically conductive Thermoplastic PolyUrethane
F	Force
f_{design}	Theoretical resonance frequency according to CAD model
FDM	Fused Deposition Modeling (trademark of Stratasys Inc.)
FFF	Fused Filament Fabrication
f_{printing}	Theoretical resonance frequency according to the dimensions of the printed part
PCB	Printed Circuit Board
PLA	PolyLactic Acid
R	Electrical resistance
RT	Room Temperature
SLA	Stereolithography

SLS	Selective Laser Sintering
T	Period of oscillations
$T_{\text{Decomposition, ETPU}}$	Decomposition temperature of ETPU filament
$T_{\text{g, ETPU}}$	Glass transition temperature of ETPU filament
TGA	ThermoGravimetric Analysis
$T_{\text{m, ETPU}}$	Melting temperature of ETPU filament
TPU	Thermoplastic PolyUrethane
T_{sample}	Surface temperature of the sample
UV	Ultraviolet
α_{ETPU}	Temperature coefficient of resistance
ζ	Damping ratio
θ	Temperature
ρ	Mass per density
$\rho_{\text{ETPU filament}}$	Electrical resistivity of ETPU filament
ρ_{Cu}	Electrical resistivity of Copper
ρ_{printed}	Electrical resistivity of printed ETPU material

List of figures

Figure 1: Conventional processes vs. AM technologies 3
Figure 2: Additive manufacturing process: the first 4 steps 4
Figure 3: SLS principle, (4) 7
Figure 4: Schematic of Digital Metal® printing process, (6) 9
Figure 5: Infill pattern for FFF 11
Figure 6: AM preferred zone according to the complexity and the quantity of the produced part, (8) 12
Figure 7: The four stages of Industrial Revolution 15
Figure 8: Schematic experimental setup for the filament resistivity measurement determination 25
Figure 9: ETPU filament electrical resistance for different lengths of the filament 27
Figure 10: PLA cube with internal ETPU wires 28
Figure 11: Resistance vs. strain test setup 30
Figure 12: Evolution of electrical resistance in printed ETPU material as a function of the strain 30
Figure 13: Evolution of electrical resistance with the temperature for the ETPU printed filament 32
Figure 14: Stress-strain curve for ETPU tensile bar 34
Figure 15: Schematic robotic arm with deformation sensor 36
Figure 16: 3 point bending test principle 36
Figure 17: Deformation sensor 37
Figure 18: 3 point bending test: experimental setup 38
Figure 19: Bending test resulting curves 39
Figure 20: Schematic image of loaded platform application 41
Figure 21: Binary sensor: "Push-sensor" 41
Figure 22: Binary sensor: "banana-shape sensor” 42
Figure 23: Simulation of the displacement of the "banana-shape" 42

Figure 24: Binary sensor test 43
Figure 25: Force sensor 44
Figure 26: Force sensor: experimental setup 45
Figure 27: Force sensor: resistance [Ω] vs. force [N] 45
Figure 28: Vibration sensor: electrical circuit for experimental testing 47
Figure 29: ETPU/PLA vibration sensor 48
Figure 30: Cantilever beam 48
Figure 31: Schematic graph of resonance frequency 49
Figure 32: Vibration sensor ETPU: experimental setup 50
Figure 33: Oscilloscope screenshot: determination of the frequency: 1 peak corresponds to 1 contact 51
Figure 34: Vibration sensor: bandwidth determination 52
Figure 35: Influence of the damping ratio on the bandwidth, (36) 53
Figure 36: Metal vibration sensor 54
Figure 37: Metal vibration sensor 55
Figure 38: Metal vibration sensor after the cleaning phase 56
Figure 39: Metal vibration sensor: sintering preparation 56
Figure 40: Metal vibration sensor after sintering 57
Figure 41: Metal vibration sensor: experimental setup 57
Figure 42: DSC curve - ETPU filament 66
Figure 43: TGA curves - ETPU filament 66

List of tables

Table 1: Comparison characteristic temperature ETPU / normal TPU 24
Table 2: ETPU filament resistivity measurement...26
Table 3: Resistivity measurements of ETPU printed filament.................................28
Table 4: ETPU printed density 33
Table 5: ETPU printed Young's modulus...34
Table 6: Metal vibration sensor: natural frequencies measurements 58

1. Introduction

1.1. Objectives

Additive manufacturing (AM), also called 3D printing, is a relatively new technology and the possibilities, benefits and drawbacks are not always well known. The objective of this thesis work was to investigate the feasibility of building components with integrated sensors using additive manufacturing technologies. It aimed to create better understanding for future development by finding a way to avoid integration of external components via the development of simple designs.

3D printing enables novel applications to be built and opens new horizons when it comes to custom-designed, low-volume parts production. Besides, the integration of 3D printed sensors into a 3D printed component might play a major role in the next industrial revolution.

The deliverable of this master thesis is a report which, based on a literature study and physical prototypes analyses, should explain the suitability to build sensor-equipped parts by additive manufacturing. The sensor should be 3D printed in or on a 3D printed component and tested.

1.2. Project plan

Firstly a literature review was conducted with the focus on the existing additive manufacturing technologies, their strengths and limitations as well as the different material possibilities. The emphasis was then on the existing embedded sensors possibilities and which physical properties can result of their use. This led to the choice of the types of sensors that have been developed within this work.

With focus on the sensors themselves, a characterisation of the chosen materials via data research and destructive or non-destructive tests has been conducted. Knowing the proper characteristics, the geometry of each type of sensor was investigated. The sensors were then 3D printed and tested before their working principle and possible applications were discussed.

2. Literature review

This chapter presents the overall AM process and investigates some of the existing technologies. A comparison between the conventional processes and the additive manufacturing technologies is given as well as a brief overview of the new concept of the Industrie 4.0 and how it motivated this work.

Finally, an overview of embedded systems in today's industry is given.

2.1. Additive Manufacturing (AM)

Also known as 3D printing, Additive Manufacturing (AM) technologies are to oppose to the subtractive manufacturing ones. Instead of removing material from a raw part, the final part is obtained by starting from a digital model and adding material (Figure 1).

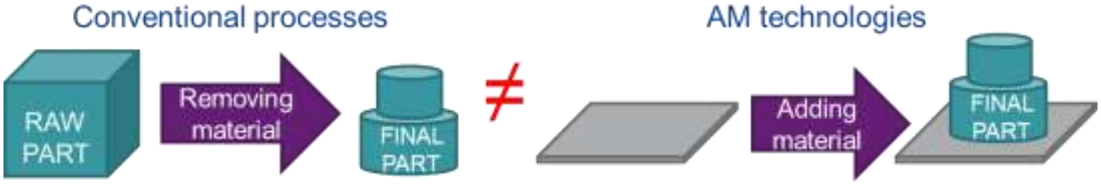

Figure 1: Conventional processes vs. AM technologies

2.1.1. Description of the AM process

In this part, the terms "AM process" or "3D printing process" do not refer to the manufacturing phase strictly but include all the steps from the creation of the 3D model to the printing itself.

Regardless which 3D printing technology will be used for the fabrication itself, every process will start in the same manner.

First of all, a 3D design must be created with the help of a CAD (Computer Aided Design) software and need to be saved in a special format: .STL.

This .STL file is then imported into the slicer software in which the designer is able to customize the settings to achieve an output as close to the requirements as possible. The slicer software will divide the 3D model into layers and create the tool path in each of them. More information about the slicer software are given in Part 3.2.The software finally generate a computer code (G-Code) and send it to the printer. Like a CNC (Computerised Numerical Control) machine tool follows a computer code to remove material, the 3D printer will follow a computer code to add material layer by layer.

When all of these 4 steps (Figure 2) are completed, the actual printing can start. The description of the process depends on the used technology. Some of them will be presented in the next part 2.1.2.

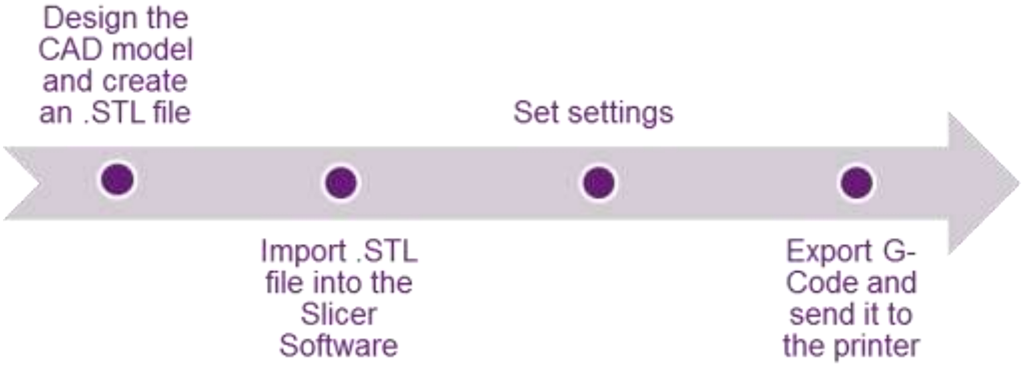
Design the CAD model and create an .STL file
Set settings
Import .STL file into the Slicer Software
Export G-Code and send it to the printer

Figure 2: Additive manufacturing process: the first 4 steps

2.1.2. Additive manufacturing technologies

3D printing is a growing sector and ameliorations are noticed every year. The list of processes exposed in this part is not exhaustive.

All the following technologies start with the 4 steps shown in the previous part: from CAD model to computer code. Only the printing technique itself changes.

Stereolithography (SLA)

Stereolithography was the first process developed for rapid prototyping. It was patented in 1986.

With this process, liquid plastic is converted into solid objects.

A SLA machine is divided in 4 parts: a tank filled with liquid photopolymer, a perforated platform that moves up and down in the tank (layer resolution = 50-150µm), an ultraviolet (UV) laser and a computer which controls both the laser and the platform.

During SLA fabrication, a thin layer of liquid photopolymer is exposed to an UV laser which scans the surface and traces the cross-section pattern. The UV-curable liquid hardens as soon as it gets touched by the laser. When the layer is completed, the build platform moves down and a new layer of photopolymer can be hardened. The process continues again and again until the printed part is finished. The final object is then removed from the platform, cleaned with a solvent to remove residues of resin and placed into an UV oven to further cure the plastic.

This technology is suitable for small parts such as presentation models master patterns and form and fit models thanks to its ability to produce highly accurate, durable objects relatively quickly (small objects in small machines take 6 to 12 hours of printing). The application industries are medical, automotive, entertainment and aerospace industries. However, the photopolymer plastics are sensitive to UV light so SLA parts are not suitable for final part applications

With this technique, support structures are needed to withstand the part during the printing. The supports are removed when the part is placed in the UV oven.

(1), (2)

PolyJet Technology

PolyJet was invented by the company Stratasys Inc.

Complex geometries with fine details and smooth surfaces can be produced thanks to this technology which consists of jetting layers of liquid photopolymer on top of each other. An UV lamp is attached to the print head and cures the material at the same time it is printed. As for the other technologies, once the layer is completed, the build platform is lowered and the process starts again for the next layer. Support material is added as the part is printed if necessary. When the part is fully formed, it is removed from the platform and cleaned. Finishing operations can be added as well.

PolyJet can be a multi-material 3D printing technology since different resins can be combined. The parts are however, like for SLA, not suitable for production applications because they do not remain stable under UV light. Best applications are master patterns, detailed prototypes or presentation models. (3)

Selective Laser Sintering (SLS)

Developed and patented in the 1980s, this technology permits to create both prototypes and final products. Sintering is the process of creating solid objects from powder using atomic diffusion under elevated temperature. During SLS, particles are fused together by a high-power laser to form a solid 3D object. The particles can be thermoplastics, ceramic powders or metal powders as well. The process is then called Direct Metal Laser Sintering (DMLS) and works for almost any metal alloy.

To create an object with SLS technology, the principle is the following (Figure 3):

- Inside the SLS machine, a levelling roller disperses a thin layer of powder material on top of the build platform,

- A computer-controlled laser pulses down on the platform and traces the cross-section of the object onto the powder according to the instruction in the G-Code (computer code). The powder grains are heated and fused together,
- Once the layer is formed, the build platform of the SLS machine moves down one step. The step value is the layer height and for SLS process it is around 100µm,
- A new layer of powder is then exposed to the laser and the process repeats, building layer upon layer until the entire object has been printed.

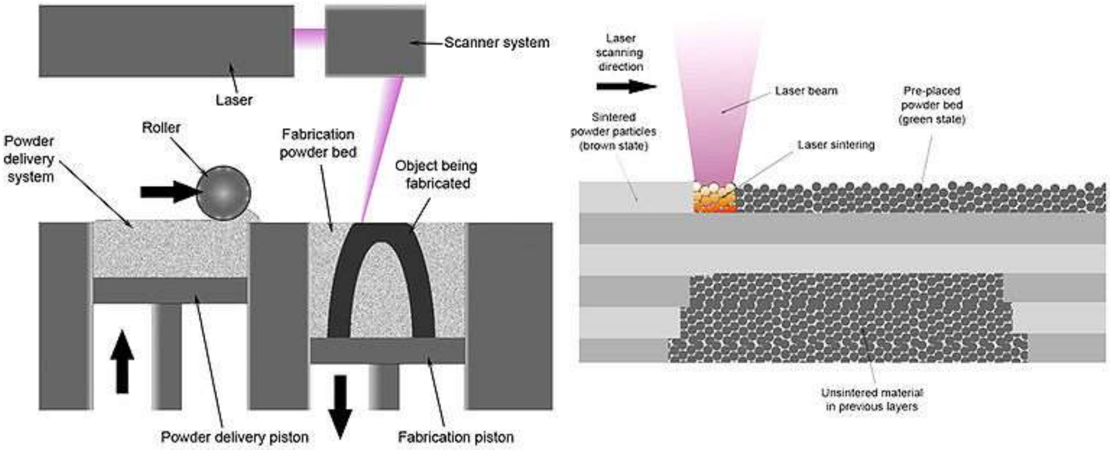
Scanner system
Laser
Roller
Powder
delivery
system
Fabrication
powder bed
Object being
fabricated
Powder delivery piston
Fabrication piston
Laser
scanning
direction
Laser beam
Pre-placed
powder bed
(green state)
Sintered
powder particles
(brown state)
Laser sintering
Unsintered material
in previous layers

Figure 3: SLS principle, (4)

With SLS, no additional supports are needed to hold the object while it is being printed. This role is played by the unsintered powder in which the part remains encased. This is even better for very complex geometries. The only thing to consider when designing a part for SLS is to have channels to clean the loose powder. It is also less time consuming than Fused Filament Fabrication and stereolithography since no supports have to be removed. Besides, no or little after processing tooling like surface finishing are required (4).

SLS parts can be strong, water and air-tight and heat resistant and parts created with DMLS have mechanical properties equivalent to cast metal parts (5).

However, because of the use of a high-power laser, it is necessary to cool down the residual heat to reduce shrinkage and improve tolerances.

Digital Metal® process

This technology is the property of Höganäs AB and the name Digital Metal® is trademarked by the company.

This process is based on precision ink-jet printing on a metal powder bed and is used to manufacture metal parts in a production scale. The resulting parts are metal components with high resolution and tolerances. Today, Digital Metal® produces mostly components in stainless steel but other materials such as titanium, silver and copper are under development. Compared to the PolyJet technology presented previously, the Digital Metal® process differs by the fact that it is not the material itself which is printed but an ink which will come and bind the metal powder grains together.

The process can be described as followed (Figure 4): a layer of powder is applied on the build platform and the print head passes over the surface, printing ink on relevant spots based on the information contained in the computer code. This is repeated layer after layer until the component is formed. After the printing, the part needs to be dried before being removed from the build box. The loose powder is then cleaned and the component is debinded and sintered to achieve the final size and strength. Some additional surface treatments can be applied to improve surface quality.

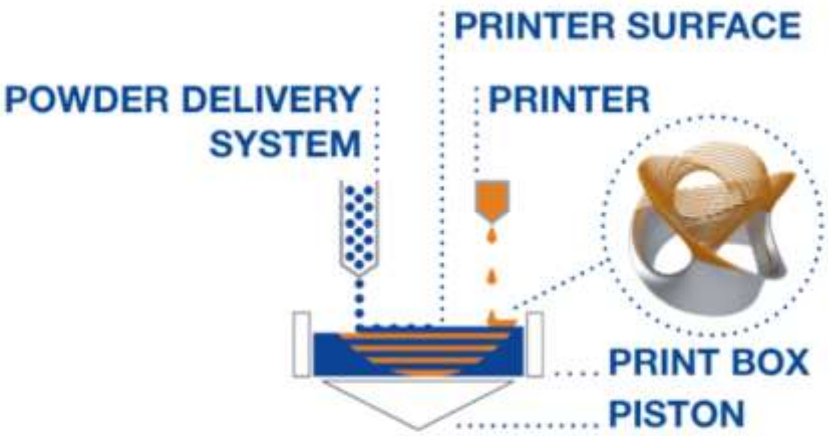

Figure 4: Schematic of Digital Metal® printing process, (6)

Because it is a powder bed based technology, the loose powder in the build box plays the role of support structures. Besides, compared to laser beam technology, the powder particles are not melted: printing occurs at lower temperature. This provides high tolerances and very high level of details. The fact that the formation happens at low temperature also facilitates the cleaning of the printed components.

With this technology, it is currently not possible to print several materials at the same time since only one type of powder is used for one printing but further development might lead to new material combinations (6).

Fused Deposition Modeling (FDM) / Fused Filament Fabrication (FFF)

Patented in 1992 by the company Stratasys Inc.[1], this technology is ideal for concept models, accurate prototypes and low-volume end-use parts. Because the term Fused Deposition Modeling and its abbreviation FDM are trademarked by Stratasys Inc., this technology will be referred to FFF for the rest of this paper.

The material used to print the 3D object is a thermoplastic filament. During the printing process, the filament is extruded and deposited by the nozzle of the print head on the build platform. When the layer is fully formed, the platform goes down and a new layer is printed. The process repeats until the final part is fully formed. The finished part is removed from the platform and the supports which were there to sustain the part during the print are removed chemically or by hand. Finally, finishing operations can be made to achieve a smoother surface. On raw FFF parts, the layers can be seen.

---

[1] http://www.stratasys.com/

Currently, this technology is one of those which offer the wider range of filament. It goes from classic ABS (Acrylonitrile Butadiene Styrene) in different colour to PLA (PolyLactic Acid) with carbon black fillers, from flexible filaments to bamboo wood filament.

If the printer is equipped with 2 printer heads it is possible to combine 2 different materials: build material and support material, same material with different colours or even 2 materials with different properties. And in theory, if more print heads are mounted together, even more materials could be printed at the same time (7).

The possibility to easily combine 2 materials with different properties was one of the reasons this technology was chosen for this thesis work.

It is interesting to notice for the rest of the project that when the infill percentage is set to 100%, it does not mean that the final part will be a solid part. As shown in Figure 5 different infill patterns can be chosen by the designer. The paths that the print head will follow create some voids in the internal structure. When it is mentioned that a part was printed “as solid as possible”, it is referring to a rectilinear infill pattern with a percentage of 100%.

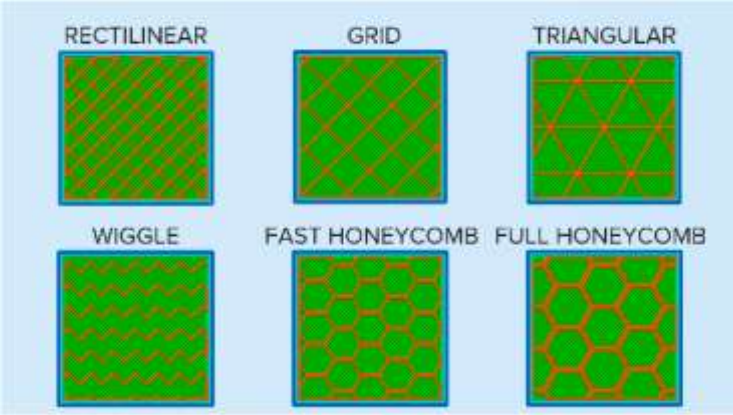

Photo by Simplify3D

Figure 5: Infill pattern for FFF

2.1.3. Comparison of AM and conventional processes

Even if comparing 3D and non-3D manufacturing is fairly asymmetric, this section will expose advantages and drawbacks of both technologies.

For traditional manufacturing technologies, the cost of a product increases as it gets more and more sophisticated (8), (9).

As shown in Figure 6, one way to reduce the costs despite enormous complexity is to produce in huge quantities. Contrariwise when talking about 3D printing, this concept is turned upside down. According to Groupe Erpro Managing Director Cyrille Vue, “the more complex and sophisticated the part is, the more interesting it is to use AM technologies compared to conventional processes” (10).

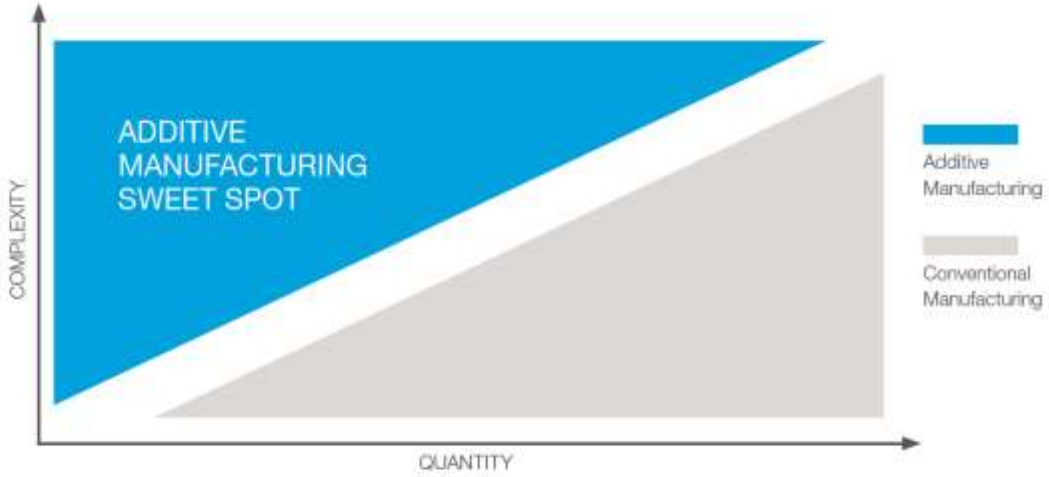

Figure 6: AM preferred zone according to the complexity and the quantity of the produced part, (8)

A 3D printer prints a complex 3D shape almost as easily as it prints a simple one. If the design can be modelled in 3D on a computer, it can be manufactured with AM, with very limited exceptions.

3D printing is suitable for all industries where complexity and individuality converge or for parts that would be impossible or too expensive to produce in any other way. AM offers the possibility to design components which include internal structures such as cooling channels and with new design considerations, one incentive of AM is the reduction of the total weight of one part. In order to do so, one component can be designed in one piece instead of assembling several smaller pieces together; fasteners and mounting components are then eliminated. The reduction of the number of parts occurs because their design is no longer restricted by the geometric limitations of moulds, dies and tool paths. Another solution to reduce the weight of a component is to make it hollow. According to a German consortium, redesigning an airplane cabin part for AM and make it lighter might save an airline $2,5 million annually in fuel costs (11).

In addition to that, additive manufacturing technologies may enable new material combinations in one unique process and the intrinsic properties (e.g. density…) of the component itself can be customized directly during the printing process. Materials which are too brittle or impossible to machine can also be used. 3D printing offers a high customization and flexibility to the designers. One application is to use 3D printing for innovative repair methodologies and predictive maintenance, where the production scale is very small and the parts are custom-designed.

Another main advantage of AM is the reduction of scrap. The material waste is kept to a minimum since only the required amount of material is used. More generally, the environmental impact of assembly and packaging of the component is lowered when using AM. Indeed if the component is printed directly in one part and not in ten, less packaging is needed, as well as less transportation energy: the parts do not need to be gathered in the assembly place in case they are manufactured in different locations. In addition to that, with AM, the CAD models are stored digitally. There is then no cost for the storage of physical moulds. This impacts also the physical products and tools inventories which are no longer needed.

Despite all these advantages, conventional processes still offer substantial benefits for certain applications. The biggest concerns of 3D printing are simplicity, quantity and speed and conventional manufacturing processes are optimised for that. AM cannot compete with traditional manufacturing technologies on an industrial scale when the volume production is high. Furthermore, when complexity of the product being manufactured is low enough, the “complexity advantage” of AM goes lost and then volume and speed requirements become decisive. For high volume production 3D printing remains too slow and complicated. Despite of all possible improvements, AM is not going to come anywhere near to catching up the production speed of conventional technologies.

Furthermore, machines excel at tight tolerances and at large components where AM has trouble. The relatively small number of available materials also limits the use of 3D printing and even if more and more technologies using metal are developed, most of the printed products are plastic. Besides, the characteristics of the final printed part could differ and there is almost always an anisotropy of the final part due to the layer by layer process.

Traditional manufacturing overall processes can be improved by providing functional and accurate 3D printed prototypes and production parts for evaluation. In that sense, AM certainly speeds up the design process. When used during the product development phase, 3D printing allows modifications and optimisations to be made in a less expensive way. It is a direct fabrication process that does not require to produce new moulds or dies for each change. Furthermore, because of the great physical distances that there can be between designers and production units, it saves time and money to develop a new product with the help of 3D printed prototypes. Design changes can then be performed and checked prior to the final part being produced and shipped. Fast iterations and failure detections early in the design cycle are possible with 3D printing without costly consequences.

3D printed models can also be used to find an optimal way to assembly the unit and then save time when it comes to the final parts.

2.2. Industrie 4.0

The manufacturing sector faces nowadays its fourth industrial revolution. This new type of industrialisation is called “Industrie 4.0”. Similar terms, such as Industrial Internet, Integrated Industry, Smart Industry or Smart Manufacturing are often used in the literature. The first industrial revolution occurred because of the mechanisation, the second because of the introduction of electrically powered mass production and the third one came with computerisation. (Figure 7). The main idea of the Industrie 4.0 is to “connect machines, work pieces and systems to create an intelligent network along the entire value chain” (12).

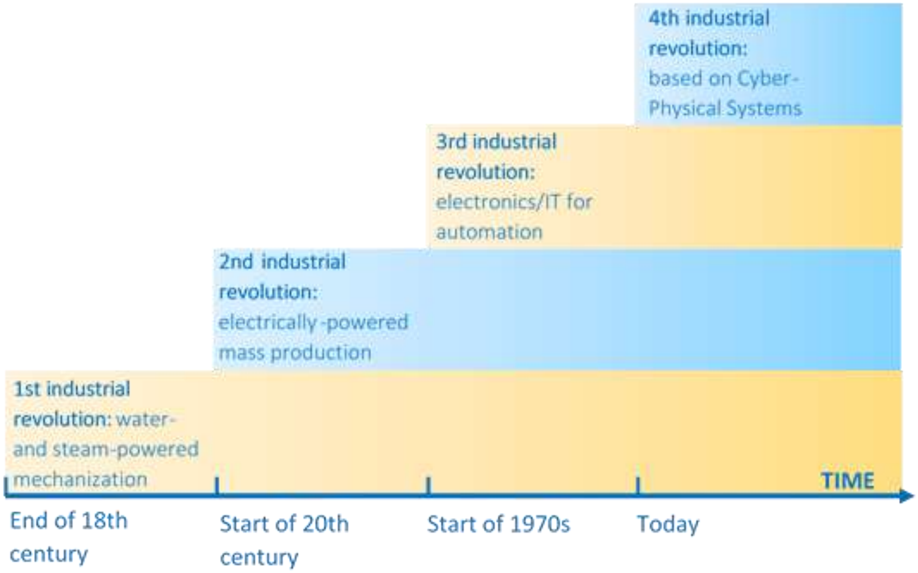
4th industrial revolution: based on Cyber-Physical Systems
3rd industrial revolution: electronics/IT for automation
2nd industrial revolution: electrically-powered mass production
1st industrial revolution: water- and steam-powered mechanization
TIME
End of 18th century
Start of 20th century
Start of 1970s
Today

Figure 7: The four stages of Industrial Revolution

From the literature, the following design principle can be noticed (12):

- Interoperability
- Digitalization
- Real-time oriented control
- Modularity

According to James E. Heppelman, CEO of PTC, people are nowadays dealing more and more with “Smart Products” and no longer with “Products”: it is the service that a product can provide which is bought by the customers, not the product itself (13). Existing basic technologies need therefore to be adapted to the specific requirements of Smart Manufacturing. At the same time, innovative solutions have to be developed. In the future, businesses will create global networks including smart machines, storage systems and production facilities in a shape of Cyber-Physical Systems (CPS). These CPS platforms will make it possible to connect people, objects and services. All of these connected entities will then be capable to communicate together via the Internet of Things and Services.

In Smart factories, information and communication technologies are used to digitize the processes. Automation engineering and digitisation may help to reduce the number of errors (14). Last-minute changes are possible as well and reactivity and flexibility lead to optimised decision-making processes. Besides, it will help with the growing customisation of products requested by the customers. In order to be flexible, an Industrie 4.0 company needs to have data that are collected and analysed in real time. In order to gather the desired data, the components need to be equipped with some measurement devices. Embedded systems can be implemented into smart products along the communication network and together with automation engineering they will exchange data about the overall situation. The status of the smart entities is permanently tracked and in case of an issue, the reaction time will then be shorter.

One easy way to integrate a sensor into a component is to directly include its fabrication in the manufacturing process of the component itself. In this sense, additive manufacturing (AM) technologies prove to be very interesting. Besides, as detailed in part 2.1.3, AM might be very advantageous when it comes to customisation of final parts.

2.3. Sensors

Layered manufacturing technologies can be applied to build smart products with sensors or integrated circuits directly placed within the component. The sensors are then as close as possible from the area of interest and real-time feedback data can be used for validating or improving designs during the prototype phase or to obtain information about the service conditions, the performance or the integrity of the component.

The integrated sensors can be used in various industries and real-time information can be strain field in the material, as well as pressure, load or temperature differences. Such sensors can also be used for tracking items on logistic lines or more surprisingly during surgical operations (15). Another advantage is that embedded sensors in a structure can monitor the physical parameters that are not accessible by ordinary sensors.

However it is not that easy to implement the embedded systems effectively. The manufacturing process to do so is most of the time a “stop, place and go” manufacturing process. This means that the printing starts, at the desired height the printing is stopped and the components inserted into the cavity, then the printing continue. In some cases, the sensors are directly put into the part. If not, place holders are inserted instead and are removed to include the sensors after the part was manufactured (16). Furthermore, the electronic parts of the sensor system is added manually (or by a robot), which may lead to some problems during the installation. With the integration of printed sensors, the manual steps are avoided and the need of an operator no longer necessary. Besides, depending on which AM technology is used, sensors have to be protected during the high-temperature deposition steps.

3. Working equipment

The main idea throughout this thesis was to combine two materials having different properties, especially different electrical properties to print a sensor. Since it is difficult to achieve when talking about metallic material, the decision was taken to work with plastic materials. Furthermore, as shown in Part 2.1.1, the FFF technology seems to be one of the best options for combining different materials easily. Several filaments are already on the market and it was possible to work with one filament which is electrically conductive and one which is not. More information about the filaments and their properties are given in Part 4.

3.1. FlashForge Dreamer

The FlashForge Dreamer is a high-end consumer desktop 3D printer which uses FFF (Fused Filament Fabrication) as printing technology. Equipped with a dual-extrusion system, this printer enables the user to print objects with two different materials without pausing the process and swapping filament each time a different colour or material is needed.

The printer also has a temperature controlled print platform. As part of this work, and to make the removal of the final parts easier, a glass plate was placed on top of the platform.

The FlashForge Dreamer offers a build volume of 230*150*140 mm and a layer resolution from 0.1 to 0.5 mm. The nozzle diameter is 0.4 mm (17).

In order to be able to print, 1.75 mm diameter filaments need to be fed into the printer. Different materials can be used but in the context of this thesis, the focus was on only two materials: PLA and ETPU. Additional details about those materials are given in the Part 4 of this paper.

3.2. Software

All the components presented in this work were designed with the help of the CAD software PTC Creo Parametric 3.0. The simulation were produced thanks to PTC Creo Simulate 3.0.

As described in part 2.1.1, once the CAD model is exported as a .STL file, a slicing software is needed. The role of this software is to "translate 3D CAD models into instructions the printer understands.” (18). For that, the software will cut the CAD model into cross-sections, also called layers and define the tool path the print heads need to follow during the printing as well as other parameters like print speed, extrusion rate and temperatures. The better the instructions, the better the result. That is why accurate 3D slicing settings are the way to a successful final print.

First used was the FlashPrint model slice driver which came with the printer but in order to be able to customise even more printing parameters, the decision was taken to switch to Simplify3D[2], which is a more advanced software. The combination of materials can be controlled in a better way and it was also an advantage because it is faster to slice a CAD file (19).

---

[2] www.simplify3d.com

4. Filaments characteristics

The main idea of this work was to combine electrically conductive and electrically non-conductive plastic filaments, i.e. PLA and ETPU. Since PLA is one of the most used materials when talking about 3D printing of plastics, the needed data for the development work have been found in the literature. For the ETPU material however, only the filament characteristics were provided by the manufacturer. In order to overcome this issue and get the data for the printed filament, destructive and non-destructive tests were run to determine its characteristic temperatures, the electrical resistivity of both the filament and the material after being printed as well as the printed density and Young's modulus.

4.1. Storage

The main enemy of 3D filament is humidity. Even if some filaments are more susceptible to degrade with the humidity than others, all do better if they are kept in a water-free environment – including the air humidity – before use or when stored for a long time. Indeed, long term exposure to a hot and/or humid environment can have damaging effect which will impact both the printing process and the quality of the final parts (20).

4.2. PolyLactic Acid (PLA)

PLA stands for PolyLactic Acid. It is a thermoplastic, i.e it becomes soft and moldable when heated and return to a solid state when cooled. This ability to melt and be processed again is what makes it prevalent in the 3D printing field. Besides, from an environmental point of view, one of the most attractive things about PLA is that itis a product derived from crops like corn-starch or sugar, which makes it bio-degradable. As an example, for an object made of PLA placed in the ocean, the degradation time is between 6 months to 2 years. For a conventional plastic, this time rises up to 500 to 1000 years. However, it is important to mention that when used in normal application conditions, PLA is very robust.

In today's industries, PLA is used for food packaging (plastic bottles) to biodegradable medical implants (sutures).

PLA has a melting temperature around T_m=160°C (21) and a glass transition temperature T_g between 60-65°C (22) at which it becomes soft and it will deform if used in environments that remain above these temperatures for long period of time (23). That is why the environment the part will be subjected to is very important to consider. PLA is a relatively hard plastic, it wears out slowly and it is easy to get a nice flat part with it. The general flexibility of the final part will mostly depend on the object's geometry rather than on the material itself (24). The thing to consider is stiffness and hardness also means that it is quite brittle. This will limit the use of PLA as material if the final part might suffer a lot of sharp collisions. Besides, it exhibits a high friction coefficient when extruding which can lead to extruder jams.

PLA can be printed at low temperatures (190-230°C, (25)) and does not require a heated build platform. However it will help the first layer to stick to the platform. An enclosed build area or an excessive ventilation is also not necessary but can be used to limit fumes.

PLA is an insulator and the PLA filament used during the experiments for this work was provided by the company Creative Tools AB[3].

Comparison PLA vs. ABS:

ABS (Acrylonitrile Butadiene Styrene) is one of the most if not the most used material when talking about 3D printing and especially FFF. It gives very sturdy and hard parts which are also suitable for machines or car industry and it has a longer lifespan. However, such properties were not the main concern for this work.

---

[3] Creative Tools AB
Slottsmöllan – 302 31 Halmstad, Sweden; www.creativetools.se

Just like PLA, ABS is electrically non-conductive but it shows some disadvantages which did not play in its favour when choosing the materials that would be used for the development of the sensors.

Whereas PLA is bio-degradable, ABS is more damaging for the environment because made out of oil-based resources. Also, it is more difficult to print. While PLA does not required a heated build platform, ABS does as well as a ventilation system. Plastic fumes are released when printing. Furthermore, ABS has a higher melting temperature (around 100°C, (26)) and needs to be printed in an enclose area and a slower 3D printer speed has to be used. This leads to a higher amount of required energy to print a model.

For these reasons, PLA was chosen as the insulator material for the development during this work. (27)

4.3. PI-ETPU 95-250 Carbon Black (ETPU)

This filament is produced in Sweden by Palmiga Innovation[4]. Made of thermoplastic polyurethane (TPU) in which carbon black fillers were added, this filament is less rubbery than standard TPU (oil based) but has several other advantages. Above all, the most interesting in the context of this work is that it is electrically conductive. In the rest of this paper, this filament will be referred to ETPU.

The filament is also flexible and wear-resistant. It possesses a decomposition temperature of 250°C and the manufacturer suggests to print it at a temperature between 210°C and 230°C, depending on the 3D printer and the print speed. The print temperature is then between the glass transition temperature and the melting point (see 4.3.1. Characteristic temperatures).

---

[4] www.palmiga.com

According to Palmiga Innovation, this filament is ideal for 3D printed dampers/shock absorbers, tires, V-belts, pens for mobile phone or tablet displays, seals, etc. (28)

4.3.1. Characteristic temperatures

Glass transition temperature, melting point and decomposition temperature.

“The glass transition temperature (T_g) of a plastics is the point at which a reversible transition of amorphous phases from a hard brittle condition to a visco-elastic or rubber-elastic condition occurs.” (29).

The melting temperature (T_m) of a solid is the temperature, under atmospheric pressure, at which it changes from solid to liquid. At the melting point the solid and liquid phases are in equilibrium.

The decomposition temperature ($T_{Decomposition}$) is the temperature at which the chemical decomposition of a polymer starts because of heat.

In order to determine those three temperature for the ETPU filament, a DSC experiment (Differential Scanning Calorimetry) as well as a TGA (ThermoGravimetric Analysis) were performed. A description of the experiment principle and the resulting curves are given in the appendix (Appendix A).

From these analyses:

$$T_{g,ETPU} = 130°\text{C}$$

$$T_{m,ETPU} = 235°\text{C}$$

$$T_{Decomposition,ETPU} = 300°\text{C}$$

Comparison ETPU / classic TPU material (30)

	ETPU	Classic TPU material
Glass transition temperature	130°C	138°C
Melting temperature	235°C	232-260°C

Table 1: Comparison characteristic temperature ETPU / normal TPU

The determination of these temperatures gives relevant information about how the filament will react when being printed as well as later on while the component will be in use.

4.3.2. Electrical resistivity

“The electrical resistivity of a material is a number describing how much that material resists the flow of electricity.” (31). A low resistivity means that the electricity can flow easily through the material and vice-versa. This property is independent of the size and shape of the piece of material.

Concerning the volume resistivity of the ETPU material, the only information provided is that the volume resistivity is less than 100 Ωcm (28). Considering that the work of this thesis is based on combining electrically conductive and non-conductive material, this is not precise enough. Therefore the resistivity for both the ETPU filament before and after printing was determined.

For both determinations, the electrical resistivity was determined at room temperature. The influence of the temperature is not considered but some tests were run to see if the temperature had an influence on the resistivity of the printed parts (see 4.3.4)

ETPU filament resistivity before printing

The filament has a circular cross-section. The electrical resistance in Ohms is measured for different lengths of the filament (Figure 8).

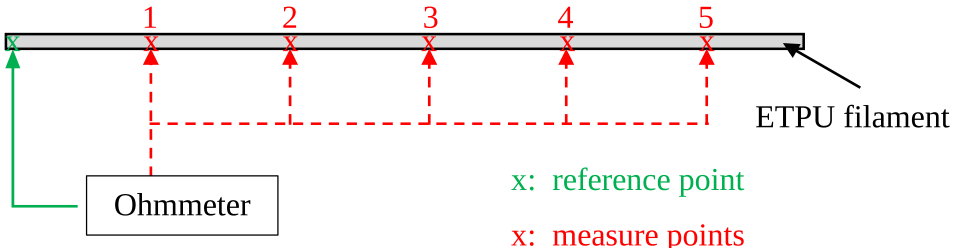
1
2
3
4
5
ETPU filament
x: reference point
x: measure points
Ohmmeter

Figure 8: Schematic experimental setup for the filament resistivity measurement determination

The resistivity is then determined from the following formula:

$$R = \rho * \frac{L}{S}$$

$$\Rightarrow \rho = \frac{R}{L} * \frac{\pi d^2}{4}$$

with ρ: resistivity [Ωcm]

R: measured resistance [Ω]

S: cross-section [cm^2]

d: diameter of the filament [cm]

L: length between measuring points [cm]

The Table 2 summarizes the different measurements and calculations.

	Measurement 1		Measurement 2	
Distance between measuring points [cm]	R [kΩ]	ρ [Ω*cm]	R [kΩ]	ρ [Ω*cm]
10	16,2	38,97	12,7	30,55
20	27,3	32,83	23,6	28,38
30	39,6	31,75	33,8	27,10
40	52,3	31,45	46,3	27,84
50	64,6	31,08	58	27,90
60	77,2	30,95	70,2	28,14
70	89,6	30,79	82,9	28,49
80	101	30,37	92,1	27,69
AVERAGE		**32,27**		**28,26**

Table 2: ETPU filament resistivity measurement

Taking the average value leads to:

$$\rho_{ETPU\ filament} = 30{,}27\ \Omega cm\ \pm 2$$

The Figure 9 shows the evolution of the electrical resistance in the material for different lengths of ETPU filament:

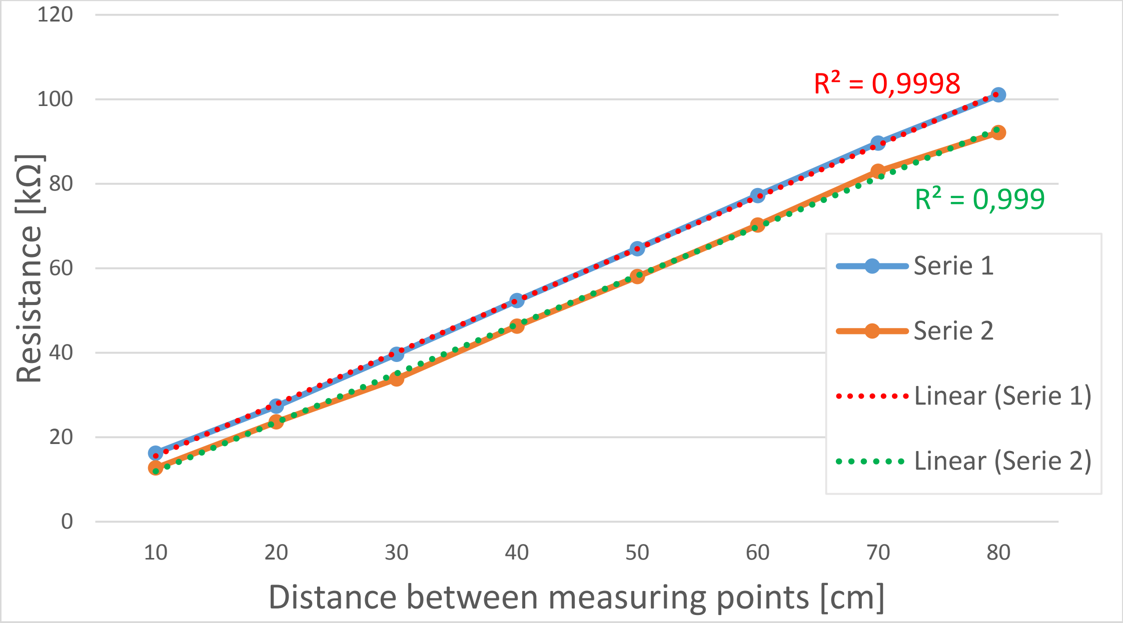

Figure 9: ETPU filament electrical resistance for different lengths of the filament

ETPU printed material resistivity

Internal wires in a cube:

Because of the manufacturing process itself, i.e. a layer by layer fabrication, the presence of resistivity anisotropy was suspected. To prove it, two samples were used. The samples were made of a support structure in PLA (dielectric) which included internal wires in ETPU (conductor). The wires were placed in X-, Y-, and Z-direction as well as within the diagonal of one face (Figure 10).

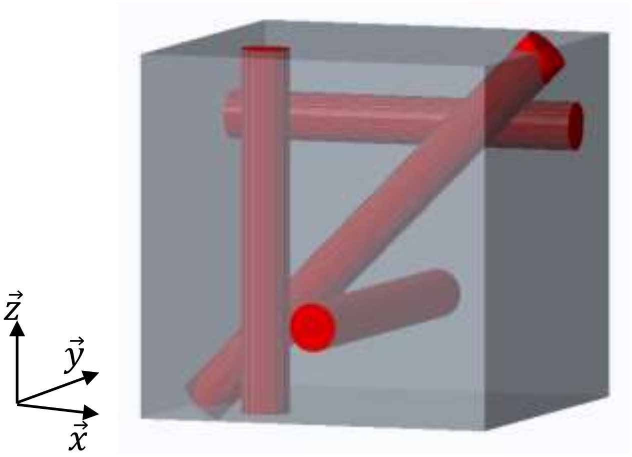

Figure 10: PLA cube with internal ETPU wires

The exact length of the wires was measured (because of tolerances between the design and the actual printed part). The diameters were however assumed correct according to the CAD model. The resistance was measured with an ohmmeter. Using the same equation than for the filament resistivity determination, the resistivity in each direction was calculated (Table 3):

	Resistivity ρ [Ωcm] Sample 1	Resistivity ρ [Ωcm] Sample 2	AVERAGE
X-direction	192,39	174,04	183,21
Y-direction	216,31	190,39	203,35
Z-direction	*No correct value*	543,02	543,02
45°-direction	*No correct value*	341,54	341,54

Table 3: Resistivity measurements of ETPU printed filament

The "no correct value" cells in the previous table mean that an infinite resistance was detected by the ohmmeter. This signifies that the wire was damaged and the current could not flow through. This problem occurred only for the wires with a big height variation (Z- and 45°-direction). This can be explain by the presence of gaps between the layers. The cross-section was so small (4mm diameter) that if air was present between layers, there would no longer be any contact between them and the wire could not carry the current anymore. In X- and Y-directions the cross-section perpendicular to Z-axis was wider so those wires were less sensitive to small air gaps. However, the second sample did not have the same problem and the resistivity in all of the 4 wires could have been calculated.

Discussion

Just as a reminder, the measured electrical resistivity of the ETPU filament was $\rho_{ETPU\,filament} = 30{,}27\ \Omega cm.$ As a comparison, the resistivity of copper is $\rho_{Cu} = 1{,}68 * 10^{-6}\ \Omega cm$ (32). Copper is a million times more conductive than the printed ETPU filament.

Furthermore, after printing, the resistivity of the ETPU material was between 180 Ωcm and 550Ωcm. This result proves first that the printing process impacts the resistivity of the material. This could be due to a change in the material structure while being printed or more likely because of the structure of the wires because of the layer by layer process and the infill pattern.

Secondly, it was obvious that talking about electrical resistivity the printed part has an anisotropy. For the same wire design, the resistivity in Z-direction was more than 2.5 times higher than in X- or Y-direction and those ones were similar. In the case of the 45°-direction, the resistivity was between the one for horizontal wires and the vertical one, which also went in the direction of this theory. This anisotropy will therefore be important to consider for the rest of this work and the printing direction will have to be chosen carefully.

4.3.3. Relation between strain and variation of electrical resistance in printed ETPU material

In order to see if the electrical resistance varies under deformation, a tensile test with extensometer was performed on a tensile bar printed in ETPU material. During the test, an ohmmeter was connected to the sample and the value of the resistance was noticed for different strains (Figure 11). The results are shown in Figure 12.

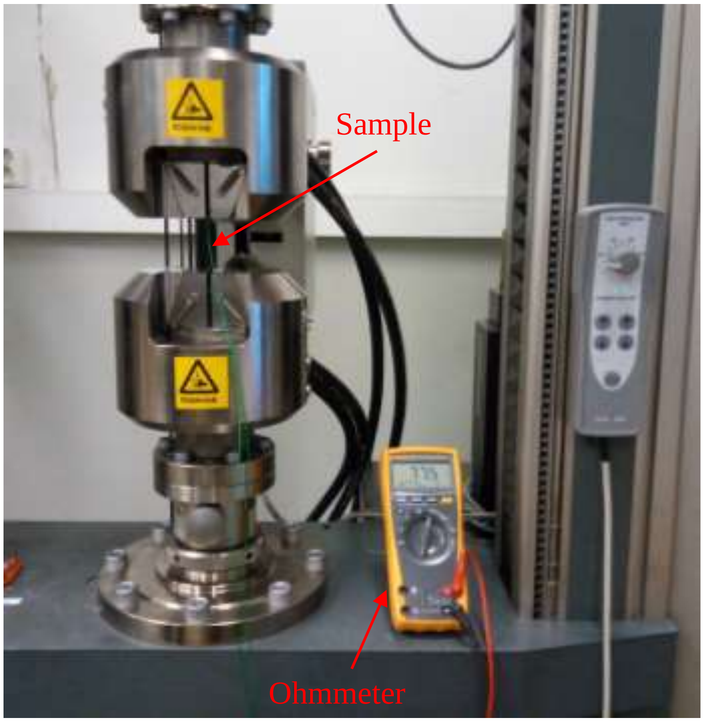

Figure 11: Resistance vs. strain test setup

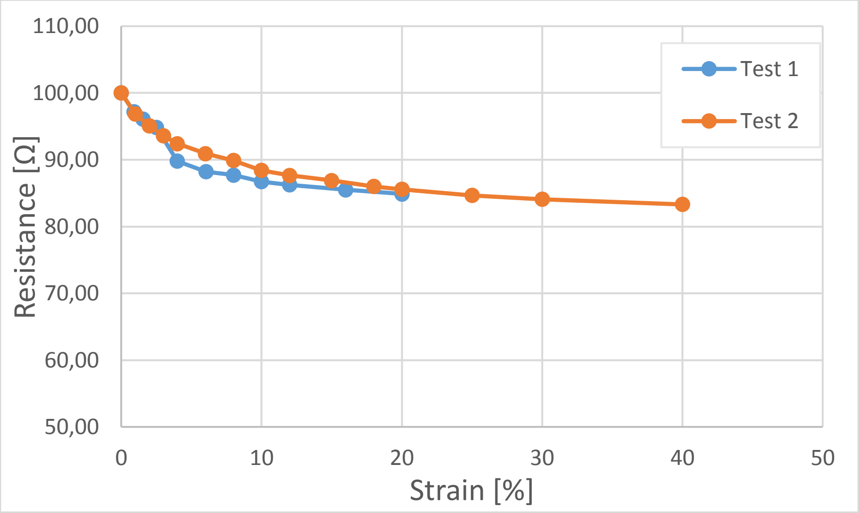

Figure 12: Evolution of electrical resistance in printed ETPU material as a function of the strain

The ohmmeter cables were inserted into two holes directly printed in the component. For this test, the holes were placed into parts of the tensile bar which were pressed in the machine jaws. It was observed that when the sample was "free" (means not pressed into the machine), the resistance was higher than when the jaws were closed but no strain was applied. This can be explained by the contact resistance between the cable and the material. Due to the cable not being perfectly straight, some air might have been between it and the material. When the jaws were closed, the material was pressed against the cable, chasing the air and leading to a better conductivity.

Result of this test was that the electrical resistance went down when the strain increased. Although more work needs to be done to fully understand the reason of this variation, the result was used for the development of the sensors.

4.3.4. Influence of the temperature on printed ETPU resistance

The rubbery consistency of the filament suggests that its electrical resistance will be influence by the temperature of its environment. In general, the variation of the resistivity with the temperature can be expressed as following (33):

$$\rho_\theta = \rho_{\theta_0}(1 + \alpha * \Delta\theta)$$

with ρ_θ: resistivity at the temperature θ [Ωcm]

ρ_{θ_0}: resistivity at the temperature θ_0 [Ωcm]

α: temperature coefficient of resistance [K^{-1}]

$\Delta\theta$: difference of temperatures [K]

The temperature coefficient of resistance symbolises the resistance change for a temperature variation of one degree. If this coefficient is positive, the resistance of the material increases with increasing temperature: the material becomes less conductive. If the temperature coefficient is a negative number, it means that the resistance decreases with increasing temperatures.

To confirm this, the resistance of a sample was measured for different surface temperatures of the sample. The evolution of the resistance with the temperature is plotted in Figure 13.

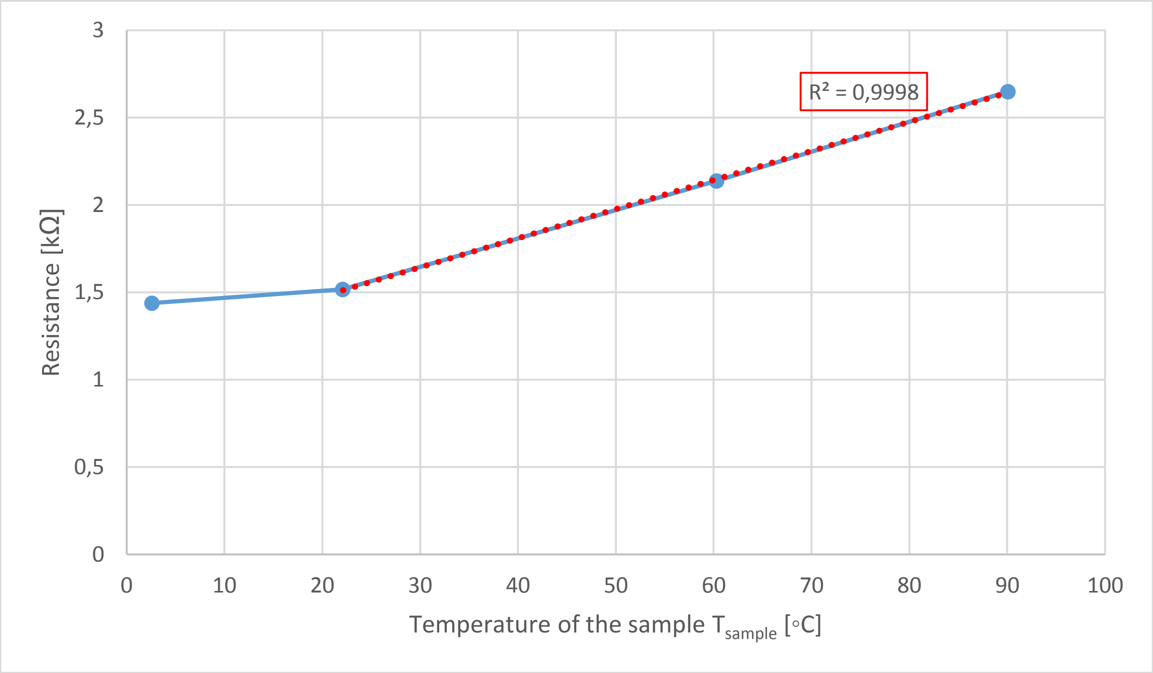

Figure 13: Evolution of electrical resistance with the temperature for the ETPU printed filament

As a reminder, the glass transition temperature of the ETPU filament is $T_{g, ETPU}$ = 155°C (Part 4.3.1).

From the previous graph, it can be said that for temperatures between 0°C and room temperature (RT), there is no noticeable difference in resistance. On the other hand, for temperatures above RT, the resistance increases linearly with the temperature: the material becomes less conductive. The previous equation is verified for the ETPU filament and the temperature coefficient of resistance can be determined:

$$\alpha_{ETPU} = 10{,}7 * 10^{-3}\ K^{-1}$$

As reference, for copper, $\alpha_{Cu} = 3{,}86 * 10^{-3}\ K^{-1}$ (32)

4.3.5. Density

According to the manufacturer data sheet, the density of the ETPU filament is 1,3 g/cm^3. However, this information is not sufficient and the density of the printed ETPU material needs to be determined. The value of the printed density is indeed necessary to calculate the theoretical natural frequency of the ETPU/PLA vibration sensor.

For the determination of the printed density, three 10mm cubes were printed as solid as possible (infill percentage = 100%, rectilinear as infill pattern), measured and weighed (Table 4)

	X-length [mm]	Y-length [mm]	Z-length [mm]	Mass [g]	Density [g/cm^3]
Cube_Printing 48	10,043	9,911	10,186	1,14	1,12
Cube_Printing 49	10,033	9,865	10,137	1,14	1,14
Cube_Printing 50	9,939	9,95	9,863	1,13	1,16

Table 4: ETPU printed density

By averaging the three previous measurement, the printed density of ETPU material is calculating:

$$d_{printed} = 1{,}14\ g/cm^3\ \pm\ 0{,}1$$

4.3.6. Module of elasticity

For the Young’s modulus E as well only the value for the filament before printing was given ($E_{\text{ETPU, filament}}$ = 12 MPa). Since the value for the printed ETPU filament is also very important, 3 samples were printed with only ETPU filament. The design of the tensile bars is based on the norm SS-EN ISO 2740:2009 and the ends were extended to provide a better grip between the sample and the machine jaws.

The strain-stress curves were used to determine the module of elasticity of the printed ETPU material. Only one curve is presented here (Figure 14) but a stress-strain curve was generated for each of the 3 samples.

The test was not run until the fracture of the sample, which was very ductile, but it was not a problem since only the Young's modulus was investigated and only the elastic domain of the curve is then necessary.

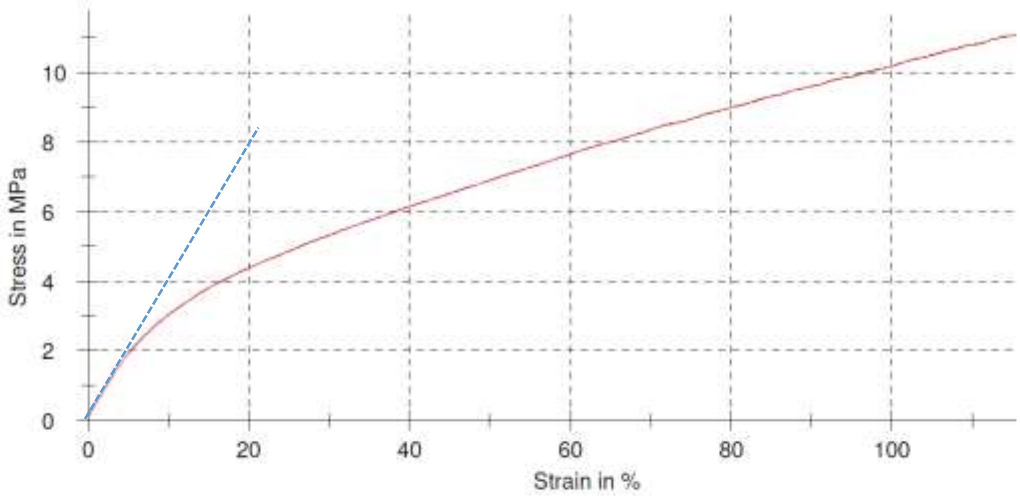

Figure 14: Stress-strain curve for ETPU tensile bar

From the resulting stress-strain curves, the values of the Young's modulus was determined (Table 5):

	Sample 1	Sample 2	Sample 3
E [MPa]	47,6	42,8	39,9

Table 5: ETPU printed Young's modulus

By averaging the values from the 3 tests:

$$E_{printed} = 43\ MPa\ \pm 3$$

5. Sensors

As mentioned in Part 2.3, the embedded systems are mostly external components which are added by an operator during the printing process. With the used FFF technology, it is effectively possible to pause the printing, insert an external part and continue to print afterwards.

However, the goal of this thesis was to demonstrate the feasibility of printing the sensor and the component all in once by combining different materials, without any outside intervention. The component, the sensor and the needed connection wires were directly manufactured together, using the possibility to combine materials and to create internal structures. Nevertheless, for this work, it was relevant to focus only on the development and the printing of the sensors themselves. Their inclusion into a more complex design was therefore out of context.

In this chapter, four types of sensors as well as their development, testing phase and a discussion regarding the feasibility and limitations are described.

5.1. Deformation sensor

The experiment of Part 4.3.3 gave the information that the electrical resistance in the ETPU is changing with strain. Based on this observation, it was interesting to develop a sensor which would be able to detect any deformation in a component. This can be applied to detect bending of a robotic arm for example (Figure 15).

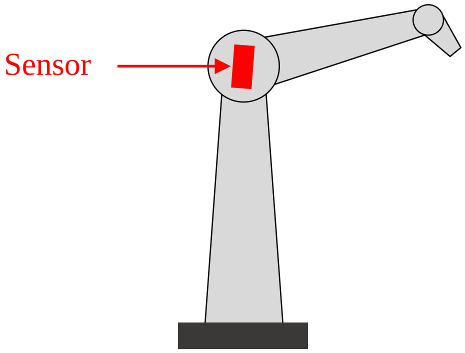

Figure 15: Schematic robotic arm with deformation sensor

Idea

The main idea is that when a load is applied on the sensor, the ductile layer will deform and a variation in the electrical resistance will be visible.

To confirm this, the following questions have to be answered:

- Will the resistance variation in the conductive layer be big enough to be detectable?
- Will the variation be repeatable?

Testing setup

To test this principle, a sample was designed and was then placed on a 3 point bending test bench (Figure 16).

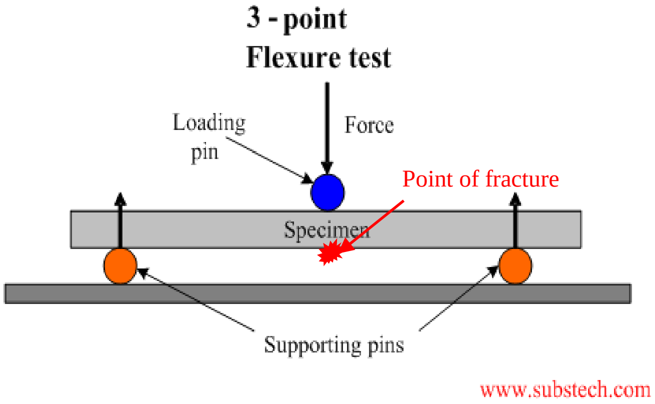
3 - point
Flexure test
Loading pin
Force
Point of fracture
Specimen
Supporting pins
www.substech.com

Figure 16: 3 point bending test principle

A specimen was placed on two supporting pins and a load was applied in the middle of it. The purpose was to determine the resistance to fracture of a material. Adapted to brittle materials, it is possible that for a ductile material the fracture does not occur. Anyway, if there would be a fracture, it would occur along the outermost edge of the sample, which was under a tensile load.

The two samples printed for this test were decomposed into a thin layer of ductile electrically conductive ETPU material (0,55mm) and a support in PLA which represented the components in which the sensor would be embedded (Figure 17). The lower stiffness of the thin layer of ETPU does not contribute much to the global stiffness of the samples. The two specimens were printed as solid as possible (rectilinear infill pattern, 100% infill).

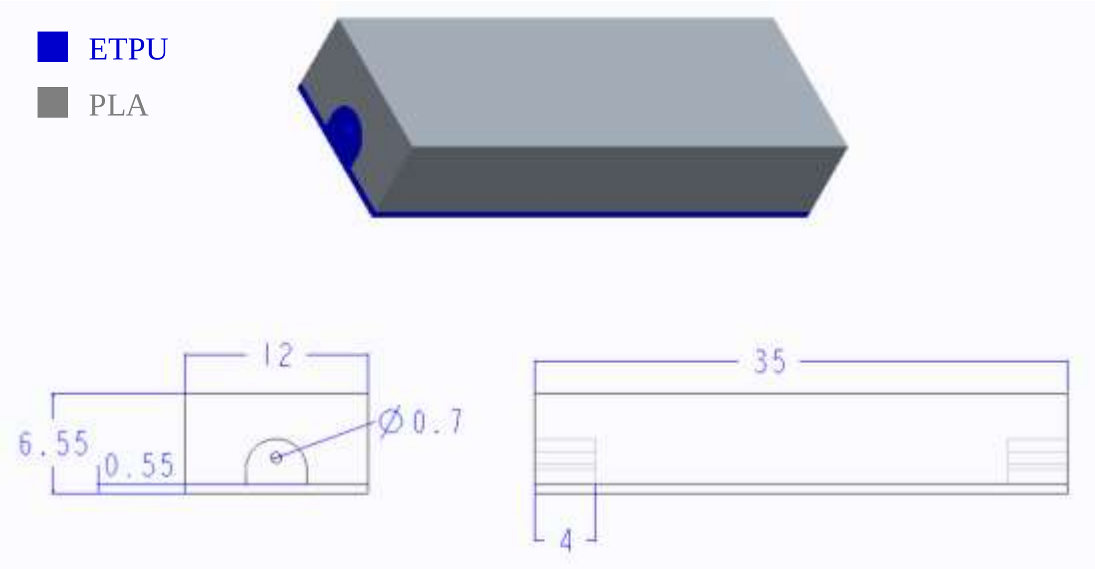

Figure 17: Deformation sensor

In order to measure the resistance within the conductive layer, an ohmmeter was connected to the sample. The ETPU thin layer also included two “ears” in which the connecting wires could be inserted. A picture of the experimental setup is given in Figure 18.

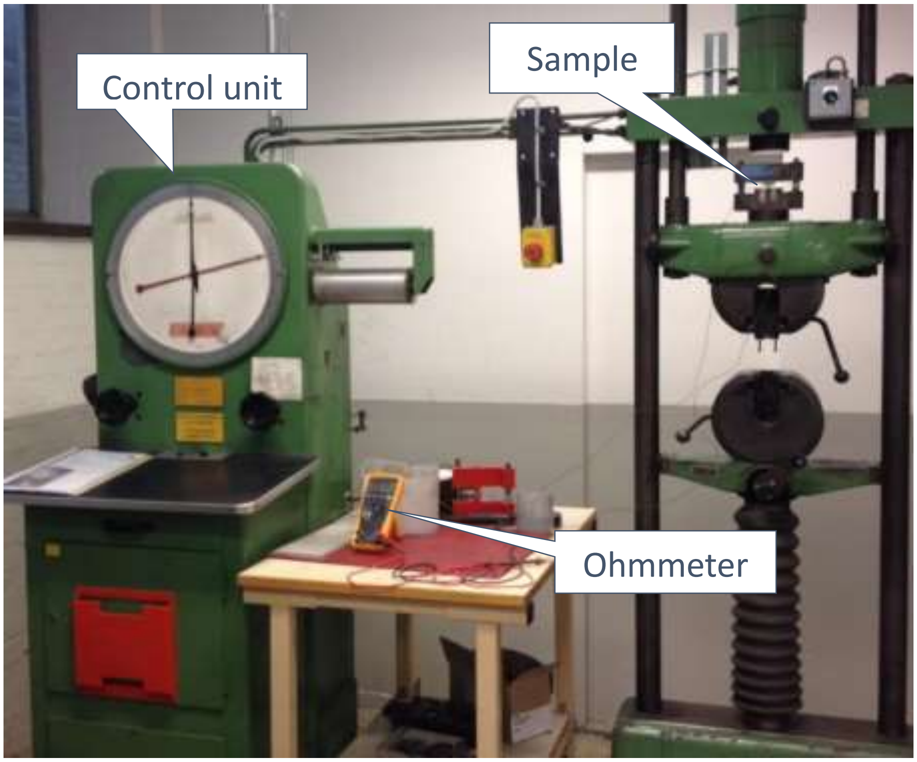

Figure 18: 3 point bending test: experimental setup

Test results

For each sample, the electrical resistance was measured with the ohmmeter when a force was applied in the middle of the specimen. It is to notice that even if called “deformation sensor”, it is not the resistance as a function of strain which is measured but as a function of the applied force. The force and the strain could then be correlated. Several load cycles were performed. As a result of the test, the measured resistance is plotted as a function of the applied force (Figure 19):

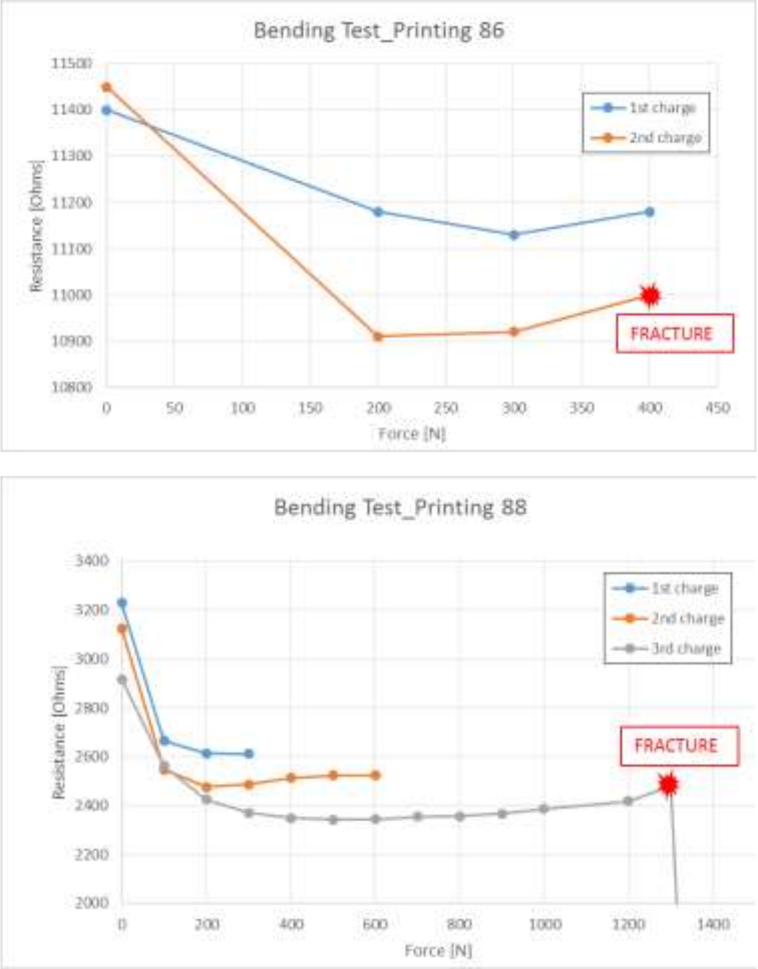

Figure 19: Bending test resulting curves

First of all, the difference in the resistance value for F=0 N for the two specimens can be explained by the fact that the samples were printed in different directions. The sample 86 (top figure) was printed with the ETPU layer directly on the build platform whereas for the sample 88 (bottom figure) the ETPU was on the top. This resulted in a stronger bond between the two materials of sample 88. This clearly shows that the positioning of the final part on the build platform had an influence.

Secondly, for both samples, the resistance went down as the applied force was increased. This fit the observation of Part 4.3.4 about the relation between the strain and the resistance variation: when the applied force was increased, the bottom layer of the sample was subjected to a tensile load and suffered a positive strain.

Furthermore, the resistance reached a plateau as the force increased. The variation of the resistance was then very difficult to see. However, it was possible to distinguish the resistance values in the first part of the curves for a force F between 0 and ~300N.

Finally, the general shapes of the curves were similar for the two samples and for the different load cycles as well, implying that there is then a certain repeatability of the measurement.

In the light of the test results, the idea exposed in this part could be confirmed and this principle be used as a deformation sensor.

5.2. Binary sensor

Sometimes, a numerical value is not necessary and a qualitative detection is enough. Therefore binary sensors were developed.

Idea

The sensors will act like a switch placed into a very simple electrical circuit. As an example of application can be named a loaded platform: if it is loaded, the circuit is closed and the current goes through and a light can eventually be displayed, if not, the circuit remains open (Figure 20).

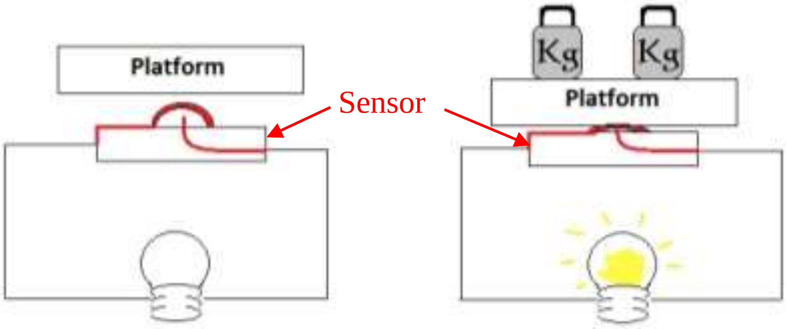
Platform
Sensor
Kg
Kg
Platform

Figure 20: Schematic image of loaded platform application

Sensors geometries

One of the main advantages of additive manufacturing is the possibility to create internal structures. That is why in addition to the material combination (ETPU and PLA) the first designed sensor includes an internal structure made of a pin and a push-button in a shape of a contact-lens (Figure 21). When the push-button is pressed, it will hit the pin which will close the circuit.

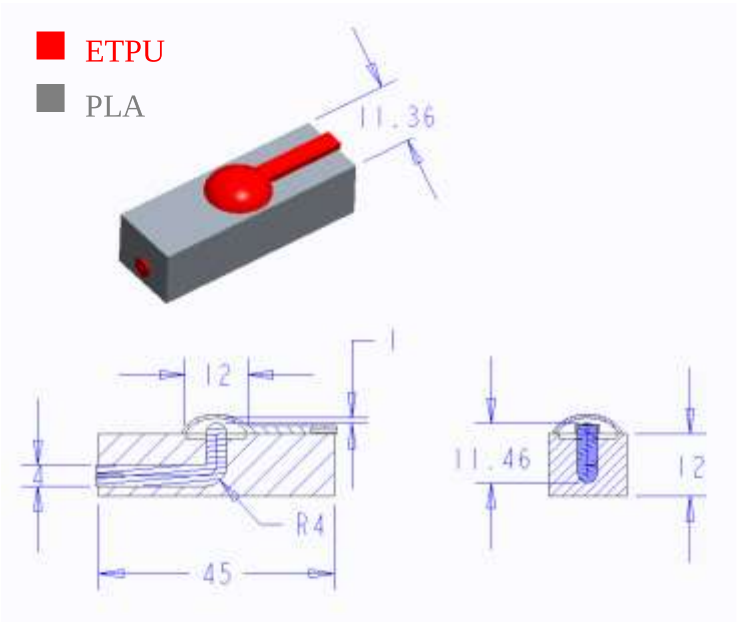
🟥 ETPU
■ PLA
11.36
12
1
4
R4
45
11.46
12

Figure 21: Binary sensor: "Push-sensor"

The second geometry combines a “banana-shaped” part and a layer printed in ETPU (Figure 22) and was elaborated with the help of PTC Creo Simulate 3.0 M020 (Figure 23).

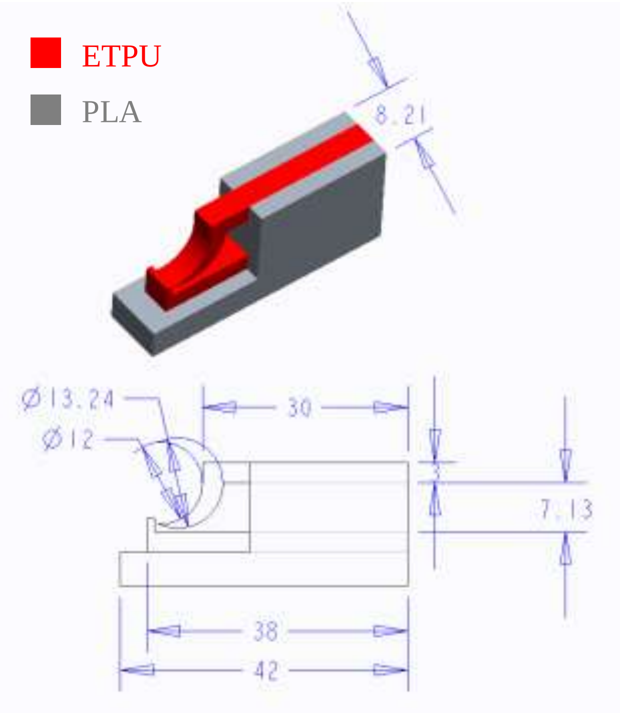
🟥 ETPU
▨ PLA
8.21
Ø13.24
Ø12
30
7.13
38
42

Figure 22: Binary sensor: "banana-shape sensor”

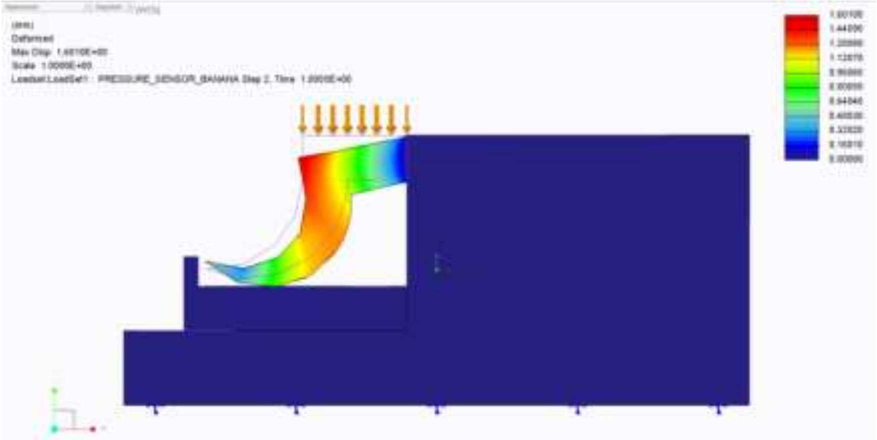
(mm)
Deformed
Max Disp 1.6010E+00
Scale 1.0000E+00
LoadSet:LoadSet1 : PRESSURE_SENSOR_BANANA Step 2. Time 1.0000E+00
1.60100
1.44090
1.28080
1.12070
0.96060
0.80050
0.64040
0.48030
0.32020
0.16010
0.00000

Figure 23: Simulation of the displacement of the "banana-shape"

The idea behind this geometry is following: when the “banana-shaped” part is pushed down, it contacts the conductive layer. When the force increases, the contact area becomes bigger and the electrical resistance changes.

Test results

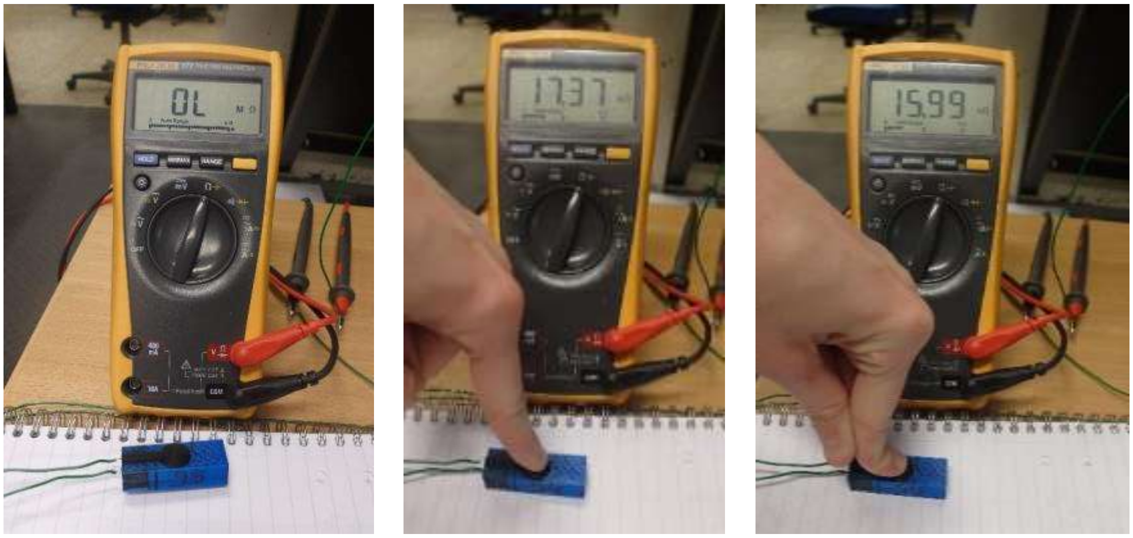

No force

F_1

$F_2 > F_1$

Figure 24: Binary sensor test

For both sensors, the tests were successful. As shown in Figure 24, when no force is applied, the ohmmeter gave an infinite resistance (left picture). On the other hand, when pressed, the conductive parts get contact in with each other and close the electrical circuit: a resistance value appeared on the ohmmeter screen (middle picture). Furthermore, it was noticed that the value of the resistance decreased when the applied force increased (right picture). This comes from the fact that the contact surface between the conductive parts increased when pushing harder. The range was however not wide. Another design may be necessary to improve the idea of an increasing contact area leading to a resistance variation. This investigation is detailed in Part 5.3.

The two sensor designs developed in this part proved their validity as binary sensors.

5.3. Force sensor

As mentioned in the previous part, the possibility to have a wider range of the contact surface variation and to be able to link the resistance values and the applied force was investigated. It was in some case needed to have numerical values. A third geometry was therefore tested: a sphere in contact with a bowl (Figure 25).

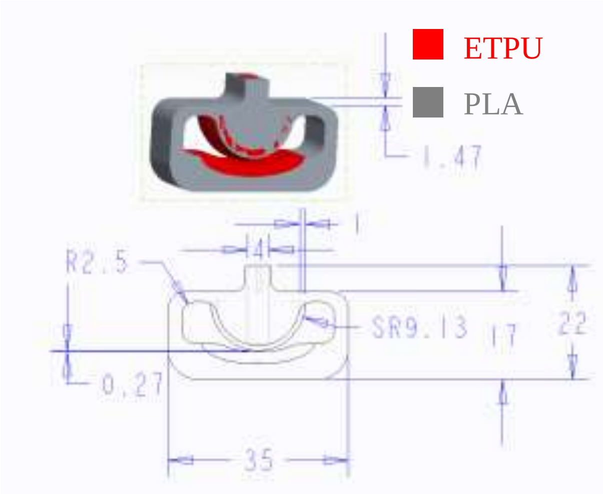

Figure 25: Force sensor

For this type of sensor, the stiffness and the stress of the housing need to be optimised to have no plastic deformation. Once again, PTC Creo Simulate 3.0 M020 was helpful to determine the proper dimensions. The idea is the following: the higher the applied force, the wider the contact area, the lower the resistance.

Testing setup

The setup was very similar to the one for the deformation sensor (Part 5.1). The force sensor was placed between two pistons and an ohmmeter was connected to it (Figure 26). As the force was applied on the top of the sensor, the electrical resistance was measured.

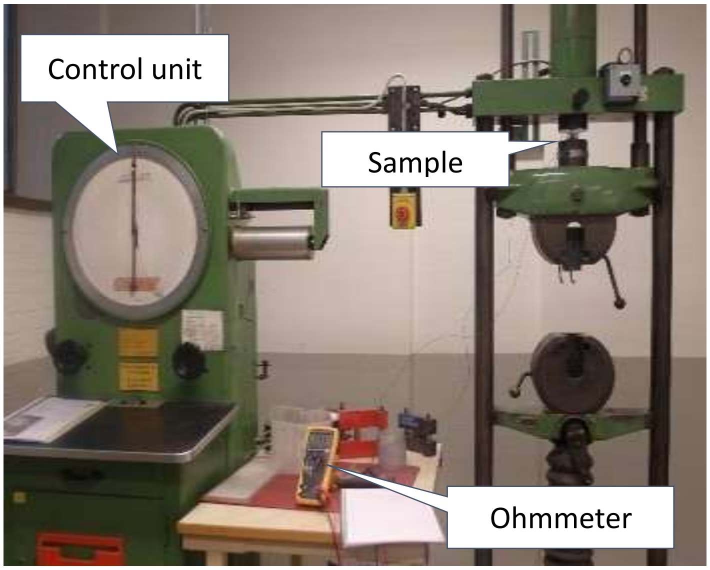

Figure 26: Force sensor: experimental setup

Testing results

Four load cycles were performed, the first three until the force reached 300N, the fourth one until no significant variation in the resistance was seen.

The resistance was plotted as a function of the applied force (Figure 27):

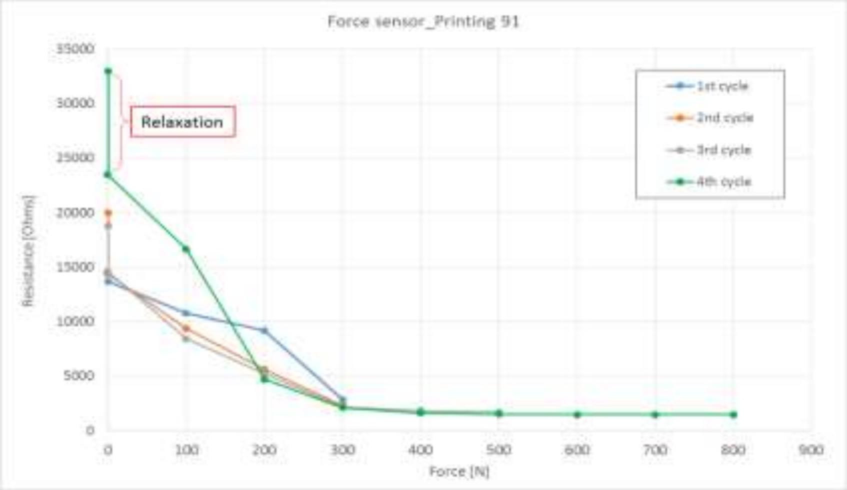

Figure 27: Force sensor: resistance [Ω] vs. force [N]

First of all, a relaxation time of about one minute was observed when unloading the sensor at the end of a load cycle: as the force was released, the resistance went relatively high and then came back slowly to a steady value. Only then the force was increased again and the next cycle started.

Secondly, the procedure was quite repeatable since the slopes of the curves had similar shape.

In the green curve (corresponding to the fourth load cycle) it is noticeable that as the force increased, the resistance reached a plateau: it was then no longer possible to detect any variation in the resistance values. But for a force between 0 and ~300N, it was easy to differentiate the values of the resistance.

The principle of this force sensor was acceptable. However, there are some issues that need to be consider. First, even if a certain repeatability was recorded, the sensor was not very accurate. Not suitable for laboratory applications it can be used at some other occasions. For example with the appropriate range of forces, it might be suitable to detect if a robotic arm is loaded or not or to detect the overload of a component. Secondly, a relaxation time was observed, which means that the sensor does not react immediately when unloaded. Finally, the printed design was a first design and optimizations can be made to improve the overall performance of the sensor.

5.4. Vibration sensor

Some dynamic systems are designed to run efficiently at one frequency and one frequency only. Such systems can be characterised in terms of one or more natural frequencies and it would be very interesting to measure this frequency while running. “The natural frequency, also called eigenfrequency, is the frequency at which the system would vibrate if it were given an initial disturbance and then allowed to vibrate freely.” (34)

Principle

The sensors developed during this work use the principle of mechanical resonance. Integrated into a bigger structure, the sensor is composed of a beam as “moving” element. The natural frequency of this beam is known. When vibrations of the beam are detected, it gives an indication about the frequency at which the complete component is shaking. It can then be used to eventually stop the system before severe damages occur because of resonance.

Testing setup

To demonstrate the principle of this type of sensor, the sensor was placed on a vibrating plate within an electrical circuit composed by a power supply and an oscilloscope (Figure 28).

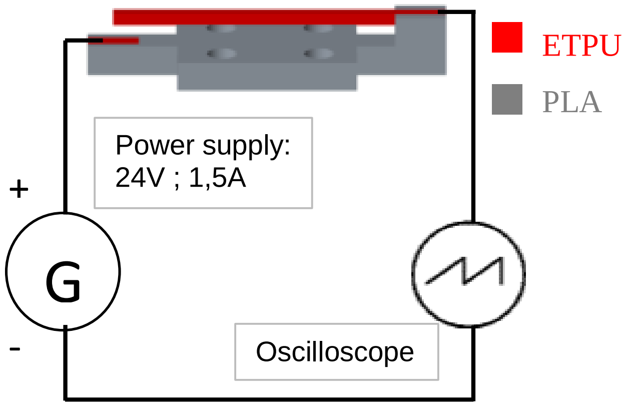

Figure 28: Vibration sensor: electrical circuit for experimental testing

The sensor will act like a switch. When the frequency of the vibrating plate reaches the natural frequency of the beam, this one will enter in resonance and vibrate with the highest amplitude. The beam will then contact a counter conductive layer and close the electrical circuit. The current is then able to go through and a voltage drop can be detected on the oscilloscope. On the oscilloscope screen, each peak corresponds to the moment when the beam hits the layer and closes the circuit (Figure 33). The vibration frequency can then be determined.

5.4.1. ETPU/PLA sensor

For this sensor, the focus was on combining conductive and non-conductive filaments. The sensor was divided into a support printed in PLA and a beam associated with a counter conductive layer made of ETPU (Figure 29).

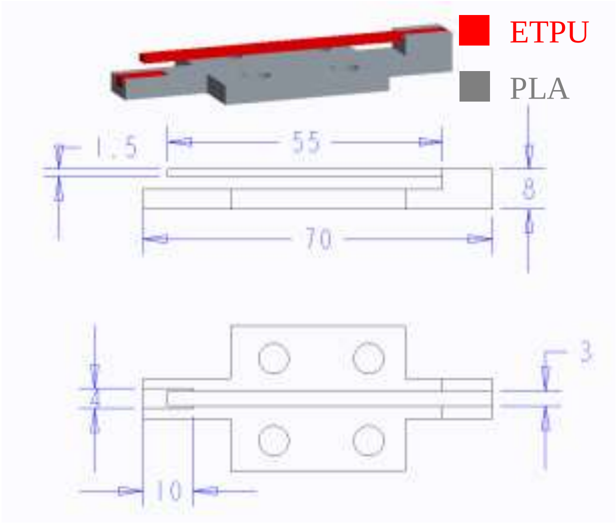

Figure 29: ETPU/PLA vibration sensor

The beam was a cantilever beam with mass per length ρ. The beam has a uniform rectangle cross-section. Furthermore, the Young's modulus E and the second moment of area I are supposed constant. The beam has a length L (Figure 30).

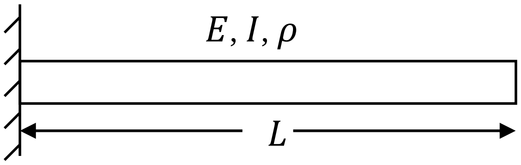

Figure 30: Cantilever beam

To be able to test the printed sensor, the limitations in the generated frequencies of the testing set-up have to be considered. It is then necessary to previously determine the theoretical eigenfrequency. There are many available methods to do so and the chosen one was the Rayleigh's method (Appendix B) (34).

This lead to the following formulae to calculate the natural frequency of a beam:

$$f_n = \frac{1}{2\pi} \frac{3{,}6639}{L^2} \sqrt{\frac{EI}{\rho}}$$

with f_n: natural frequency [Hz]

L: beam length [m]

E: Young's modulus [Pa]

I: second moment of area [m^4]

ρ: mass density [kg/m]

Knowing the fundamental bending frequency of the beam, the dimensions – length, width, height – can be chosen.

Test results

The vibration of the beam was detectable. However this design can be qualified as a "sensor" only if there are vibrations of the beam around its resonance frequency f_0 (Figure 31).

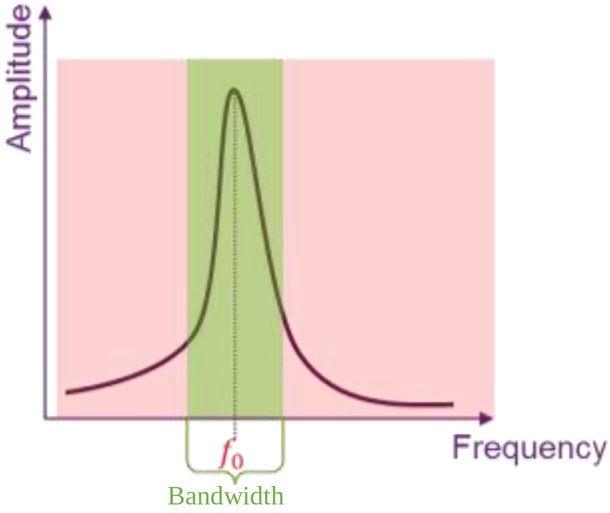

Figure 31: Schematic graph of resonance frequency

Measurements were executed in order to determine how wide the bandwidth was where vibrations could be detected with the oscilloscope. The Figure 32 shows the experimental setup:

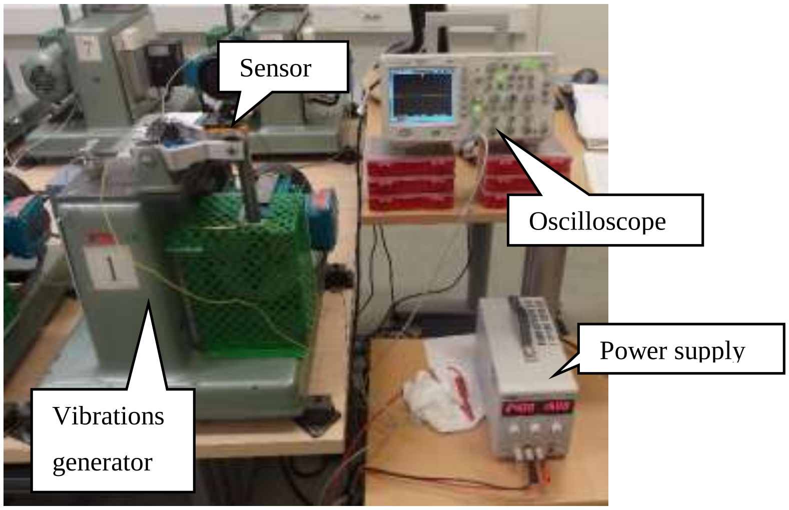
Sensor
Oscilloscope
Power supply
Vibrations generator

Figure 32: Vibration sensor ETPU: experimental setup

The procedure was following:

- Starting at low frequency, the frequency of the vibrating plate was increased until peaks were visible on the oscilloscope screen and the corresponding frequency was determined. An example of the calculation is given in Figure 33:

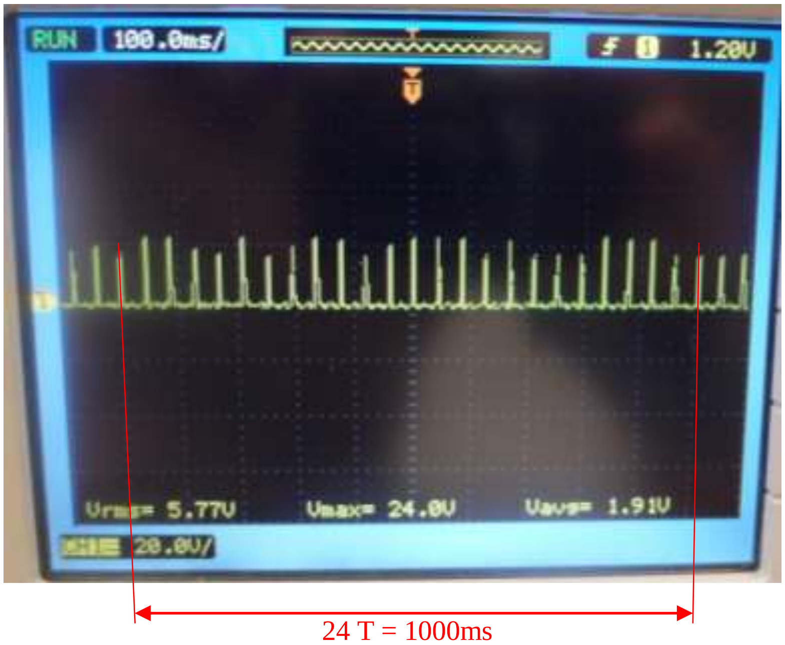
RUN
100.0ms/
1.20V
Urms= 5.77V
Umax= 24.0V
Uavg= 1.91V
20.0V/
24 T = 1000ms

Figure 33: Oscilloscope screenshot: determination of the frequency: 1 peak corresponds to 1 contact

$$24T = 1000ms$$

$$T = 46{,}67 * 10^{-3}s$$

$$f = \frac{1}{T} = 21{,}43\ Hz$$

with T: period of the oscillations [ms]

f: frequency of the oscillations [Hz]

- The frequency of the vibrating plate was then augmented again until the peaks on the oscilloscope screen disappeared. The corresponding frequency was determined similarly.

This procedure was repeated six times for each of the two identical samples. The measurements are summarized in Figure 34:

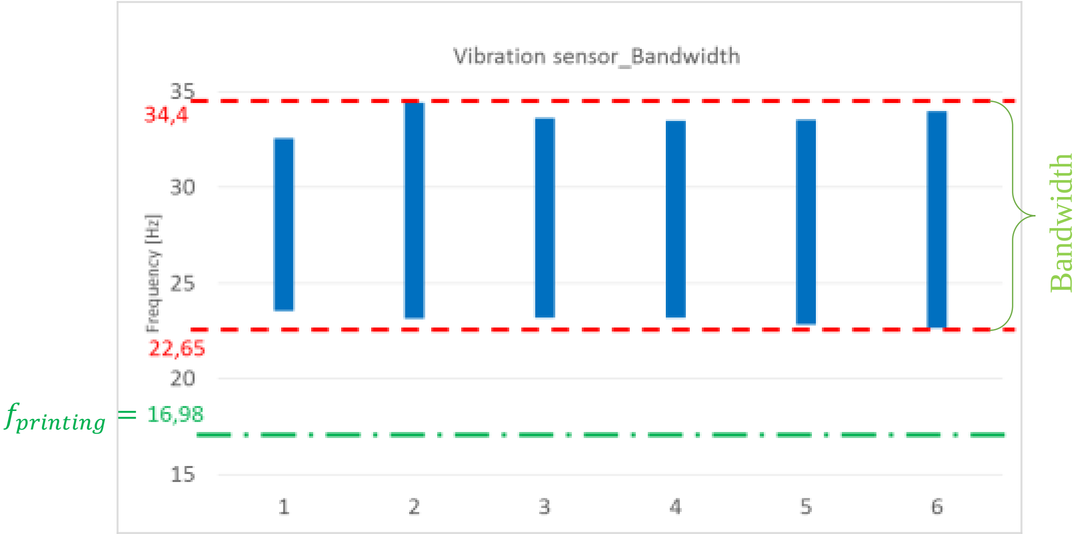

Figure 34: Vibration sensor: bandwidth determination

Comparison of theoretical and measured value

The theoretical value of the natural frequency according to the CAD model dimensions is:

$$f_{design} = 16{,}29\ Hz.$$

Because of the tolerances between the model and the printed part, the dimensions of the real beam were measured and the theoretical eigenfrequency was then:

$$f_{printing} = 16{,}98\ Hz.$$

When comparing these two theoretical resonance frequencies and the measured bandwidth, it is noteworthy that the values are different. There is a ratio of about 1,5 between the theory and the measurement and the experimental values are higher than the theoretic ones.

First, the bandwidth of the sensor beam is relatively wide. This can be due to the fact that the ETPU material seems to have a high damping ratio ζ. As shown in Figure 35, the higher the damping ratio, the wider the bandwidth.

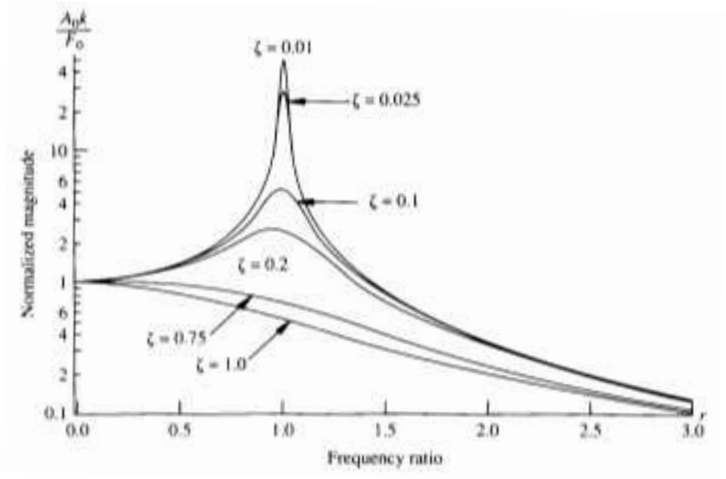

Figure 35: Influence of the damping ratio on the bandwidth, (36)

Furthermore, the difference between the theoretical values and the measurement can be attributed to the fact that the Rayleigh's method used to determine the theoretical frequency only gives an approximation, based on the approximation displacement function used for the calculation. In addition to that, the measured material properties of the printed ETPU might not be accurate. It was proven that the printing process does influence these properties. The Young's modulus of the ETPU beam might be different from the one determined in Part 4.3.6. In the sensor beam, due to of the thin design, it is possible that more voids were present. Once again, 100% infill percentage does not mean that the final part is a fully solid part.

5.4.2. Metal sensor

As mentioned earlier in this paper, the concept of the sensors was based on the combination of conductive and non-conductive parts. However, additive manufacturing of metal parts is also a growing sector and some consequent improvements may occur in the near future. Therefore the possibility to print a metal vibration sensor was investigated.

The technology used for this development was the Digital Metal® process (Part 2.1.2). Stainless Steel 316L powder was used for this fabrication and a Printed Circuit Board (PCB) was used as insulator (Figure 36).

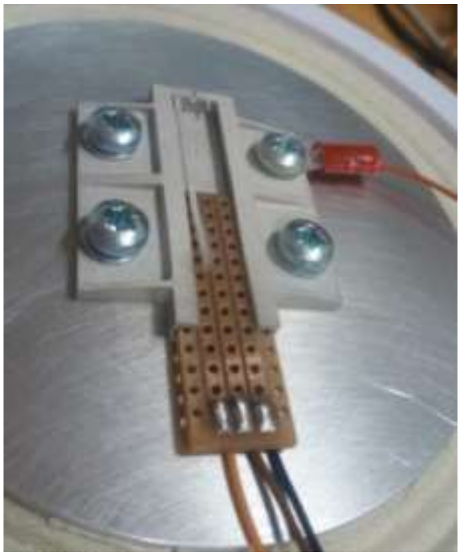

Figure 36: Metal vibration sensor

[redacted]

[redacted]

The principle remains the same as for the ETPU/PLA sensor but this time, three beams were combined (Figure 37).

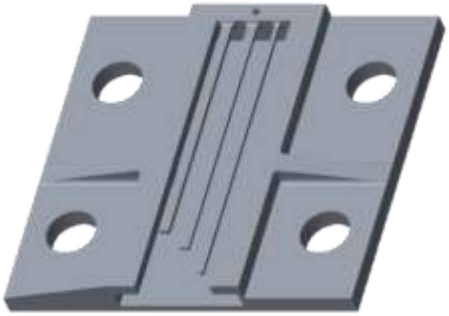

Figure 37: Metal vibration sensor

The beams had different dimensions. Consequently they have different natural frequencies. By putting them all together in one sensor, it offers the possibility to detect various vibration frequencies with only one system.

Manufacturing troubleshooting

As explained in Part 2.1.2, once the part is printed, it needs to be cleaned from loose powder and sintered to achieve the final size and strength. Including the operator time for cleaning the component and preparing it for the sintering process, it takes approximately 36 hours for the whole manufacturing.

The printing itself was successful. However, the very thin design of the beams led to some broken beams during the cleaning phase. The loose powder was blown away and sometimes the air flow just broke beam as well. The Figure 38 shows a complete sensor altogether with its three beams after the cleaning phase.

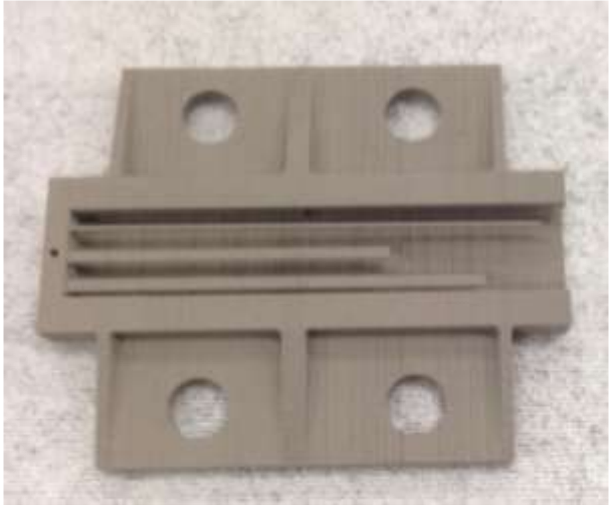

Figure 38: Metal vibration sensor after the cleaning phase

Because of the thin beams, several options were tried for the sintering process in order to preserve as many beams as possible. Alumina powder with different grains sizes was used as a support material for the beams not to bend because of the gravity. The disposition is shown in Figure 39:

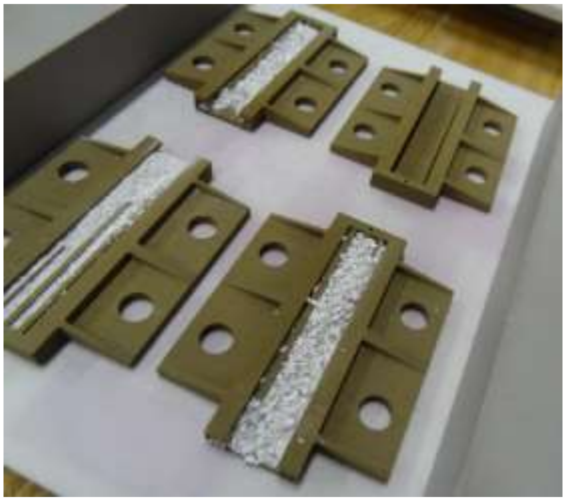

Figure 39: Metal vibration sensor: sintering preparation

After sintering, the remaining beams as well as the flat surface of the sensor were quite distorted. During the sintering phase, the component usually shrinks about 20% and thin designs and walls are less susceptible to retain their shape (Figure 40).

However, this vibration sensor was able to be tested in spite of the distortion.

Testing setup

Because the Young’s modulus was much higher for the metal than for the ETPU material, the stiffness of the beam was higher as well as its natural frequency. Therefore a new testing setup was necessary, in order to generate oscillations which were big enough at the desired vibration frequency (Figure 41).

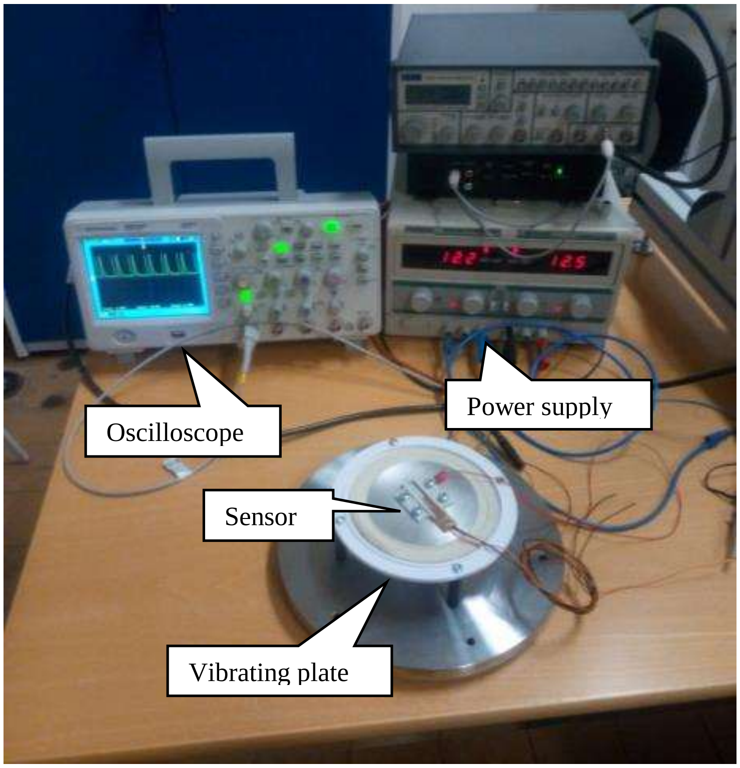

Figure 41: Metal vibration sensor: experimental setup

Test results

The testing procedure for the determination of the natural frequencies of the beams was the same than for the ETPU/PLA vibration sensors. The measurements were made on four different sensors, since some beams were broken (Table 6).

Theoretical frequency [Hz]	Sample A	Sample B	Sample C	Sample D
$f_1 = 200,47$	//	~170	//	~160
$f_2 = 399,06$	//	//	//	$319 < f <335$
$f_3 = 304,47$	$269 < f < 275$	~255	$270 < f < 288$	~250

Table 6: Metal vibration sensor: natural frequencies measurements

Unlike the ETPU/PLA vibration sensor, the theoretical eigenfrequencies of the beams are higher than the experimental ones. This could be justified by the higher damping coefficient of the ETPU material: the damping coefficient will indeed lower the natural frequency of the beam.

Besides, the bandwidth for the metal sensor seems to be narrower. The lower damping ratio could once again be an explanation to that.

Finally, even if the distortion of the beam may have an influence on the resonance frequency, the most important to take into consideration are the properties after printing. It is hard to say if it is enough but the printing does have a profound influence on the final properties.

Optimization

The principal issues that were observed can be explained by the very small cross-section of the beams as well as their relatively long length. This because the sensors were designed to trigger as the frequency of the vibrating plate reached the resonance frequency of the beam. Thus it is essential that the fundamental frequencies of the beams were within the possible frequencies range according to the testing setup.

To overcome this problem and make sure that the beams first would survive the manufacturing process and then were straight, a change in their geometry could be made. It could be a wider-cross section as well as going from a cantilever beam to a cantilever beam with an end-mass. The correspondent resonance frequency would then be given by the following equation (35):

$$f_n = \frac{1}{2\pi}\sqrt{\frac{3 * EI}{(0{,}2235\rho L + m) * L^3}}$$

with f_n: natural frequency [Hz]

L: beam length [m]

E: Young's modulus [Pa]

I: second moment of area [m^4]

ρ: mass density [kg/m]

m: mass of the end-mass [kg]

This would of course affect the natural frequency but it may sometimes be necessary. The optimization could be used for calibration tools or if the space around the sensor is restricted. Besides it would not be a problem as long as the natural frequency is within the range of the frequencies that have to be detected.

6. Discussions and conclusions

New possible designs for 3D printed sensors were developed. All these designs were printable after the optimum print settings were found. The designs were categorised into four types of sensors.

Whether it was for deformation measurement, as binary sensors, force sensors or to detect vibrations of a system, the printability and the combination of ETPU and PLA material investigated in this thesis has proven its suitability for the creation of 3D printed sensors. During this thesis it was revealed that it is possible to use a combination of different materials to create smart parts with embedded systems thanks to additive manufacturing.

However there are some issues for 3D printed parts that need to be dealt with. It was proven that the printing direction has a profound influence on the final part properties. Choices which will influence the results have to be made in the pre-printing phase and that is where experience would help to narrow down their impact.

Besides, a further investigation regarding the ETPU material structure is needed to fully understand what happens within the material when it is subjected to strain. The design of the force sensor exposed in this paper could as well be enhanced in order to enlarge the possible applications with a better accuracy. Finally, for both vibration sensors, different geometries of the beams might be interesting to test and new design for the metal vibration sensor could be developed in order to overcome manufacturing troubleshooting.

This work only presents four sensor principles but this is not exhaustive. Tilt sensors as well as temperature gradient sensors possibilities could also be interesting to investigate. Furthermore, with the help of new filament possibilities and multi-material emerging AM technologies - including multi-metal 3D printing - it will not stay restricted to the use of plastics.

References

1. Elizabeth Palermo, “What is Stereolithography?”, http://www.livescience.com/38190-stereolithography.html, 16 July 2013
2. Stratasys Inc., https://www.stratasysdirect.com/solutions/stereolithography/
3. Stratasys Inc., https://www.stratasysdirect.com/solutions/polyjet/
4. Elizabeth Palermo, “What is Selective Laser Sintering?” http://www.livescience.com/38862-selective-laser-sintering.html, 13 August 2013
5. Solid Concepts, “Selective Laser Sintering (SLS) Technology”, www.youtube.com, 15 May 2013
6. Höganäs AB, http://www.hoganas.com/en/business-areas/digital-metal/technology/
7. Stratasys Inc., https://www.stratasysdirect.com/solutions/fused-deposition-modeling/
8. Stratasys Direct Inc., “How 3D printing will continue to transform manufacturing”, White Paper, 2015
9. “The Achilles' Heel of 3D Printing”, Innovation Investment Journal, 30 December 2012
10. Gimélec, “Industrie 4.0 - Les leviers de la transformation”, p. 21, 2014
11. Terry Wohlers, “Making product by using additive manufacturing”, Manufacturing Engineering, April 2011
12. Mario Hermann, Tobias Pentek, Boris Otto, “Design Principles for Industrie 4.0 Scenarios: a literature review”, Working Paper, p. 10, 2015
13. Gimélec, “Industrie 4.0 - Les leviers de la transformation”, p. 48, 2014
14. Sara Zaske, “ Germany's vision for Industrie 4.0: The revolution will be digitised “, 23 February 2015
15. J.F.I. Paz, J. Wilbig, C. Aumund-Kopp, F. Petzoldt, “RFID transponder integration in metal surgical instruments produced by additive manufacturing”, Powder Metallurgy, Vol. 57, pp. 365-372, 5 December 2014

16. Sriram Praneeth Isanaka, Frank Liou, " The Applications of Additive Manufacturing Technologies in Cyber-Enabled Manufacturing Systems", 15 August 2012
17. FlashForge 3D Printer, http://www.ff3dp.com/index.php/3d-printers/dreamer-3d-printer.html
18. Simplify3D, https://www.simplify3d.com/
19. Nick Lievendag, http://nicklievendag.com/simplify3d-vs-makerbot-desktop/, 15 July 2014
20. Luke Chilson, http://www.protoparadigm.com/news-updates/the-difference-between-abs-and-pla-for-3d-printing/, 26 January 2013
21. MATBASE, http://www.matbase.com/material-categories/natural-and-synthetic-polymers/agro-based-polymers/material-properties-of-polylactic-acid-monomere-pla-m.html
22. http://www.matbase.com/material-categories/natural-and-synthetic-polymers/agro-based-polymers/material-properties-of-polylactic-acid-monomere-pla-m.html
23. http://www.matterhackers.com/
24. "3D Filament Guide: Popular 3D Printing Filaments", www.blog.pinshape.com, 22 September 2015
25. Creative Tools, http://www.creativetools.se/filament/pla-se/eco-pla-1-75mm-svart-2kg, 2015
26. http://www.makeitfrom.com/material-properties/Acrylonitrile-Butadiene-Styrene-ABS/
27. http://www.absplastic.eu/pla-vs-abs-plastic-pros-cons/?_sm_au_=iVVrQRRfnMZTRNJ5, 25 May 2013
28. Palmiga Innovation, www.palmiga.com
29. BASF Polyurethanes GmbH, "Thermoplastic Polyurethane Elastomers (TPU) - Technical Information", 2011
30. Lubrizol Advanced Materials Inc., "Technical Data sheet Isoplast 202 LGF40 ETPU", 2009

31. Michael B. Haeney, “Chapter 7: Electrical Conductivity and Resistivity”, Electrical measurement, signal processing and displays, 2004
32. http://hyperphysics.phy-astr.gsu.edu/hbase/Tables/rstiv.html
33. All about circuits, Temperature Coefficient of Resistance. Vols. 1 - Direct Current (DC), 12: Physics of Conductors and Insulators, Textbook, 2015
34. Dr Yi-Kue Lee, “Rayleigh’s method”
35. Tom Irvine, “Bending frequencies of beams, rods and pipes, Revision S”, 2012
36. Steen Krenk, “Classical Mechanics in brief”, Division of Mechanics, Lund University. March 1997

Appendices

Appendix A

Melting point and glass transition temperature

“The glass transition temperature (T_g) of a plastics is the point at which a reversible transition of amorphous phases from a hard brittle condition to a visco-elastic or rubber-elastic condition occurs.” (29).

The melting temperature of a solid is the temperature, under atmospheric pressure, at which it changes from solid to liquid. At the melting point the solid and liquid phases are in equilibrium.

In order to determine the glass transition temperature $T_{g,ETPU}$ and the melting temperature $T_{m,ETPU}$ of the filament, a DSC experiment is run (Differential Scanning Calorimetry). The principle of this procedure can be shortly explain as follow: a sample and a reference are placed into the machine and heated up. The temperature is scanned and the amount of energy necessary to keep both the sample and the reference at the same temperature is measured. When the sample starts to melt, more energy is needed to continue to increase the temperature. From the following DSC curves (Figure 42):

$$T_{m,ETPU} = 235°\mathrm{C}$$

$$T_{g,ETPU} = 130°\mathrm{C}$$

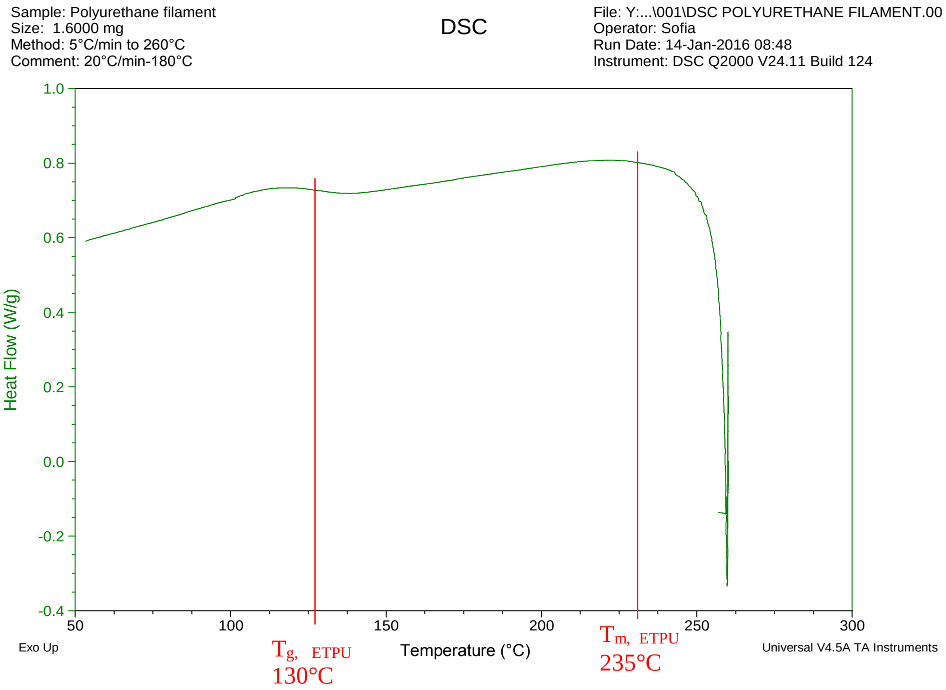

Figure 42: DSC curve - ETPU filament

Decomposition temperature

The decomposition temperature is determined thanks to a TGA experiment (ThermoGravimetric Analysis). The TGA instrument measure the weight of the sample while increasing linearly the temperature. As the temperature increases, the components of the sample are decomposed and the weight percentage of each mass change is measured. It results a graph of the mass loss as a function of the temperature (Figure 43). For the ETPU filament:

$$T_{Decomposition,ETPU} = 300°C$$

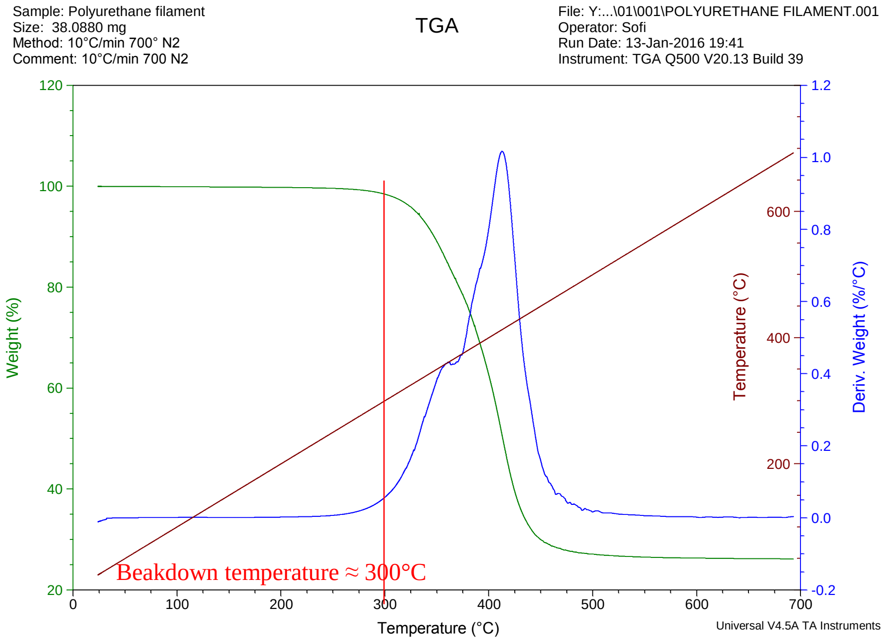

Figure 43: TGA curves - ETPU filament

Appendix B

Derivation and calculation eigenfrequency of cantilever beam:

According to the Rayleigh's method, the following equation can be satisfied only if the vibrating system frequency equals the natural frequency (34):

$$T_{max} = U_{max} = total\ energy\ of\ the\ system$$

with T: kinetic energy

U: potential energy.

This method necessitates an approximation displacement function and yields an upper limit of the true natural frequency. Knowing the fundamental bending frequency of the beam, the dimensions - length, width, height – can be chosen.

For this sensor design, the beam is a cantilever beam with mass per length ρ. The beam has a uniform rectangle cross-section. Furthermore, the Young's modulus E and the second moment of area I are supposed constant. The beam has a length of L.

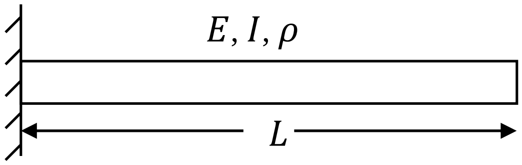

Governing differential equation:

For all the theoretical calculation, the assumption of Euler/Bernoulli is supposed to be valid.

$$-EI\frac{\partial^4 y}{\partial x^4} = \rho\frac{\partial^2 y}{\partial t^2}$$

with E: Young's modulus [Pa]

I: second moment of area [m^4]

ρ: mass density [kg/m]

Boundary conditions:

At the fixed end $x = 0$, the boundary conditions are:

- Zero displacement: $y(0) = 0$
- Zero slope: $\frac{dy}{dx}_{x=0} = 0$

At the free end $x = L$, the boundary conditions are:

- Zero bending moment: $\frac{d^2y}{dx^2}_{x=L} = 0$
- Zero shear force: $\frac{d^3y}{dx^3}_{x=L} = 0$

Approximation displacement function:

A quarter cosine function is chosen:

$$y(x) = y_0\left[1 - \cos\left(\frac{\pi x}{2L}\right)\right]$$

The proposed solution meets both the boundary conditions at the fixed end but only one at the free end: for the zero bending moment. This solution is however accepted as an approximate solution for the deflection shape.

Using the Rayleigh's method, the natural frequency can be calculated but before, the kinetic energy and the potential energy must be determined.

Kinetic energy:

$$T = \frac{1}{2}\rho\omega_n^2 \int_0^L y^2\, dx$$

with T:kinetic energy [J=kg.m^2.s^{-2}]

ρ: mass density [kg/m]

ω_n: pulsation [rad.s^{-1}]

L: beam length [m]

By substitution,

$$T = \frac{1}{4}\rho\omega_n^2 y_0^2 L\left[3 - \frac{8}{\pi}\right]$$

Potential energy:

$$U = \frac{EI}{2}\int_0^L \left(y''(x)\right)^2\, dx$$

with U: potential energy [J=kg.m^2.s^{-2}]

E: Young's modulus [Pa]

I: second moment of area [m^4]

L: beam length [m]

By substitution,

$$U = \frac{\pi^4}{64} * \frac{EI}{L^3} y_0^2$$

The kinetic energy and the potential energy are then equalised:

$$\frac{1}{4}\rho\omega_n^2 y_0^2 L\left[3 - \frac{8}{\pi}\right] = \frac{\pi^4}{64} * \frac{EI}{L^3} y_0^2$$

Using the relation between the pulsation and the frequency $\omega_n^2 = (2\pi f_n)^2$, the natural frequency can be expressed:

$$f_n = \frac{\pi}{8L^2}\sqrt{\frac{EI}{\rho(3-\frac{8}{\pi})}}$$

$$f_n = \frac{1}{2\pi}\frac{3{,}6639}{L^2}\sqrt{\frac{EI}{\rho}}$$

with f_n: natural frequency [Hz]

L: beam length [m]

E: Young's modulus [Pa]

I: second moment of area [m^4]

ρ: mass density [kg/m]

For a beam with a rectangle cross-section, the second moments of area, in m^4, with respect to x- and y-axis are:

$$I_x = \frac{bh^3}{12}$$

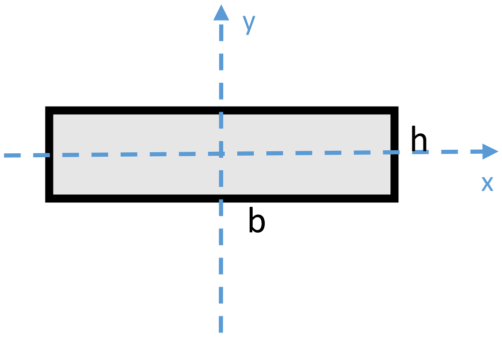$$I_y = \frac{hb^3}{12}$$